

An annual assessment of air quality with the CALIOPE modeling system over Spain

J.M. Baldasano^{a,b}, M.T. Pay^a, O. Jorba^a, M. Piot^a, P. Jiménez-Guerrero^c

^a*Earth Sciences Department, Barcelona Supercomputing Center, Barcelona, Spain*

^b*Environmental Modeling Laboratory, Technical University of Catalonia, Barcelona, Spain*

^c*Department of Physics, University of Murcia, Murcia, Spain*

Abstract

The CALIOPE project, funded by the Spanish Ministry of the Environment, aims at establishing an air quality forecasting system for Spain. With this goal, CALIOPE modeling system was developed and applied with high resolution (4 km x 4 km, 1hr) using the HERMES emission model (including emissions of resuspended particles from paved roads) specifically built up for Spain. The present study provides an evaluation and an assessment of that air quality modeling system, namely WRF-ARW/HERMES/CMAQ/BSC-DREAM8b for a full year simulation in 2004 over Spain. The evaluation focused on the capability of the model to reproduce the temporal and spatial distribution of gas phase species (NO₂, O₃, and SO₂) and particulate matter (PM₁₀) against ground-based measurements from the Spanish air quality monitoring network. The evaluation of the modeling results on an hourly basis showed a strong dependency of the performance of the model on the type of zone (urban, suburban and rural) and the dominant emission sources (traffic, industrial, and background). The O₃ chemistry is best represented in summer, when mean hourly variability and high peaks are generally well reproduced. The mean normalized error and bias meet the recommendations proposed by the United States Environmental Protection Agency (US-EPA) and the European regulations. Modeled O₃ shows higher performance for urban than for rural stations, especially at traffic stations in large cities, since stations influenced by traffic emissions (i.e. high NO_x emissions) are better characterized with a more pronounced daily variability. NO_x/O₃ chemistry is better represented under non-limited-NO₂ regimes. SO₂ is mainly produced from isolated point sources (power generation and transformation industries) which generate large plumes of high SO₂ concentration affecting the air quality on a local to national scale where the meteorological pattern is crucial. The contribution of mineral dust from the Sahara desert through the BSC-DREAM8b model helps to satisfactorily reproduce episodic high PM₁₀ concentration peaks at background stations. The model assessment indicates that one of the main air quality-related problems in Spain is the high level of O₃. A quarter of the Iberian Peninsula presents more than 30 days exceeding the value 120 µg m⁻³ for the maximum 8-hr O₃ concentration as a consequence of the transport of O₃ precursors downwind the Madrid and Barcelona metropolitan areas, and industrial areas and cities in the Mediterranean coast.

Corresponding author at: Earth Science Department, Barcelona Supercomputing Center-Centro Nacional de Supercomputación (BSC-CNS),

Jordi Girona 29, Edificio Nexus II, 08034 Barcelona, Spain. Tel.: +34 93 413 77 19; Fax: +34 93 413 77 21.

Email address: jose.baldasano@bsc.es (J.M. Baldasano)

Keywords: Model evaluation, Air quality, Spain, High resolution, O₃ Exceedances.

1. Introduction

In Europe, human health issues caused by degraded air quality have been extensively studied (Brunekreef and Holgate, 2002; Gryparis et al., 2004; Pénard-Morand et al., 2005), and have motivated the increase of monitoring infrastructures and modeling capabilities. In this sense, the European Commission (EC) and the U.S. Environmental Protection Agency (US-EPA), among others, have shown a great interest in air pollution transport and dynamics. Both entities have set ambient air quality standards for acceptable levels of O₃ (US-EPA, 1991; European Commission, 2008), NO₂, SO₂, PM_{2.5} and PM₁₀ in ambient air. According to the European regulations (European Commission, 2008), local to regional air quality models are useful tool to assess and understand the dynamics of air pollutants, to forecast the air quality, and to develop emission abatement plans and alert the population when health-related issues occur.

Air pollution limit values and allowed numbers of exceedances established by the European Commission (2008) are still exceeded in the atmospheric boundary layer in Europe and, particularly, in Spain (de Leeuw and Vixseboxse, 2010). Despite improvements due to European legislations, particulate matter and ground-level ozone remain important pollutants affecting human health (EEA, 2009a,b, 2010). The impact of these European policies on the pollutant levels was assessed by the Clean Air For Europe (CAFE) programme (Amann et al., 2004; Cuvelier et al., 2007).

The CALIOPE project, funded by the Spanish Ministry of the Environment, (Ministerio de Medio Ambiente y Medio Rural y Marino), aims at establishing an air quality forecasting system for Spain (Baldasano et al., 2008a). CALIOPE (Fig. 1) encompasses a high-resolution air quality forecasting system, namely WRF-ARW/HERMES-EMEP/CMAQ/BSC-DREAM8b, being applied to Europe as a mother domain: 12 km x12 km, 1 hr (Pay et al., 2010) as well as to Spain as the nested domain: 4 km x 4 km, 1 hr. Such high resolution of the modeling system is made possible by its implementation on the MareNostrum supercomputer hosted by the Barcelona Supercomputing Center-Centro Nacional de Supercomputación (BSC-CNS). Four Spanish research institutes compose the CALIOPE project: the BSC-CNS, the “Centro de Investigaciones Energéticas, Medioambientales y Tecnológicas” (CIEMAT), the Institute of Earth Sciences Jaume Almera of the “Centro Superior de Investigaciones Científicas” (IJA-CSIC) and the “Centro de Estudios Ambientales del Mediterráneo” (CEAM). In this project both experimental and operational modeling aspects are conducted by the BSC-CNS and CIEMAT while IJA-CSIC and CEAM lead the data monitoring part for the evaluation processes. Current forecasts are available through <http://www.bsc.es/caliope>.

To date, a total of 23 model systems routinely simulate the air quality over Europe, with seven systems also operated in the forecasting mode (Menut and Bessagnet, 2010). Due to the episodic nature of dust outbreaks, the representation of these events cannot be well simulated with solely the information of aerosol boundary conditions (Jiménez-Guerrero et al., 2008a; Menut and Bessagnet, 2010). Vautard et al. (2005a) showed that simulated aerosol loadings, using the current knowledge on aerosol mechanisms, may be underestimated by up to 30-50 % if only anthropogenic sources are taken into account. Among the seven operational systems CALIOPE is the unique system including the contribution of Saharan dust on an hourly basis. In addition, CALIOPE includes the High-elective Resolution Modelling Emission System (HERMES, see Baldasano et al., 2008b) specifically applied with high-resolution over Spain.

Several studies investigated air quality concerns over selected areas in Spain (San José et al., 1999; Jiménez-Guerrero et al., 2008b; Vivanco et al., 2008) or over the entire Peninsula (Baldasano et al., 2008a; Jiménez-Guerrero et al., 2008a; Vivanco et al., 2009). Most models ran with horizontal cell resolution of 18 km x 18 km or coarser for domains covering the Spanish territory. CALIOPE now uses a 4 km x 4 km cell resolution to simulate the Iberian Peninsula domain. Such high resolution is a key factor to accurately simulate air pollution issues, especially over complex topography (Jiménez et al., 2006) and meteorology patterns (Baldasano et al., 1994; Millán et al., 2002a) in southern Europe.

The present paper provides a quantitative performance assessment of the CALIOPE modeling system to simulate the air quality in Spain (gas phase and particulate matter). As the HERMES emission database was compiled for the year 2004 the evaluation was carried out over this year. The performance of the modeling system is evaluated by means of comparisons with ground-based observations from the Spanish network here in after referred to as “RedESP” (source: CEAM, see Fig.2). The model dynamics are evaluated together with the corresponding statistics. The results are then compared to model performance goals and criteria. This study intends to warrant the suitability of CALIOPE over Spain for air quality concerns and forecast.

Section 2 describes the different models used in the CALIOPE system, the observational dataset and the statistical parameters calculated. Section 3 analyses the system results against available observations for the year 2004 and the modeled annual distribution of NO₂, O₃, SO₂ and PM₁₀. A discussion about the exceedances of O₃ during summertime is shown in Section 4. The conclusions are presented in Section 5.

2. Methods

2.1 System Description

The CALIOPE air quality system is a state-of-the-art modeling framework currently under further development. As shown in Fig. 1, CALIOPE is a complex system that integrates a meteorological model (WRF-ARW), an emission processing model (HERMES), a mineral dust atmospheric model (BSC-DREAM8b), and a chemical transport model (CMAQ) together in an air quality forecasting system.

The Advanced Research Weather Research and Forecasting (WRF-ARW)

model v3.0.1.1 (Michalakes et al., 2004; Skamarock and Klemp, 2008) provides the meteorology to the chemical transport model. For the Spanish domain WRF-ARW is configured with a grid of 397 x 397 points corresponding to a 4 km x 4 km horizontal resolution and 38 σ vertical levels with 11 characterizing the planetary boundary layer (PBL). The model top is defined at 50 hPa to resolve the troposphere-stratosphere exchanges properly.

The Models-3 Community Multiscale Air Quality Modeling System (Models-3/CMAQ, Byun and Ching, 1999; Binkowski, 1999; Byun and Schere, 2006), v4.5 is used to study the behavior of air pollutants from regional to local scales, due to its generalized coordinate system and its advanced nesting grid capability. According to the work by Jiménez et al. (2003) the photochemical mechanism used in this study is the Carbon Bond IV mechanism (CBM-IV, Gery et al., 1989). It includes gas, aerosol and heterogeneous chemistry. The production of sea salt aerosol (SSA) is implemented as a function of wind speed and relative humidity (Gong, 2003; Zhang et al., 2005) through the AERO4 aerosol module. This module comprises the following aerosol components: nitrate, sulfate, ammonium, elemental and organic carbon, soil, sodium, and chlorine. Unspecified anthropogenic aerosols and aerosol water are additionally kept as separate components. Aerosols are represented by a trimodal aerosol distribution (Aitken, accumulation and coarse mode) using the ISORROPIA thermodynamic equilibrium model (Nenes et al., 1998), each of them assumed to have a lognormal distribution (Binkowski and Roselle, 2003). Secondary inorganic aerosols (SIA) are generated by nucleation processes from their precursors to form nitrate ammonium and sulfate aerosols. Secondary organic aerosol (SOA) can be formed from aromatics (anthropogenic organic aerosols) and terpenes (biogenic organic aerosols, Schell et al., 2001). Aerosol deposition is treated by a second-generation deposition velocity scheme (Binkowski and Shankar, 1995; Venkatram and Pleim, 1999). For a more complete description of the processes implemented in CMAQ see Byun and Schere (2006).

The CMAQ horizontal grid resolution corresponds to that of WRF. Its vertical structure was obtained by a collapse from the 38 WRF layers to a total of 15 layers steadily increasing from the surface up to 50 hPa with a stronger density within the PBL.

In order to provide adequate boundary and initial conditions to the IP domain the CALIOPE model system was initially run on a regional scale (12 km x 12 km in space and 1 hour in time) to model the European domain (mother domain). Chemical boundary conditions for this domain were provided by the global climate chemistry model LMDz-INCA2 (Hauglustaine et al., 2004; Folberth et al., 2006). A detailed evaluation of the European simulation was recently presented in the companion paper by Pay et al. (2010). A one-way nesting was then performed to retrieve the meteorological and chemical conditions for the IP domain (see Fig. 1).

As highlighted by Lam and Fu (2009) stratospheric amounts of O₃ interpolated from global chemical models and provided to the chemical lateral profiles may cause problems since CMAQ does not include a cross-tropopause exchange mechanism. Following their suggestion the stratospheric contribution of O₃ from the mother domain was suppressed from the chemical boundary conditions to avoid inconsistent intrusions of stratospheric O₃ down to the surface.

The HERMES model (Baldasano et al., 2008b) uses information and state-of-

the-art methodologies for emission estimations. It calculates emissions by sector-specific sources or by individual installations and stacks. Raw emission data are processed by HERMES in order to provide a comprehensive description of the emissions to the air quality model. Emissions used for Spain are derived from the aggregation in space from 1 km x 1 km dataset to 4 km x 4 km. HERMES was recently updated with the following: Inclusion of agriculture and livestock emissions (SNAP10 sector, see Baldasano et al., 2008b), correction of emission factors of isoprene in winter, improvement in the spatial distribution of biogenic emission and population density via the use of the Corine Land Cover information at a 250 m-resolution, introduction of emissions from the road traffic sector in small cities (SNAP07 sector). In addition, since a decade, emissions of resuspended particles from paved road have received an increasing attention. Field measurements showed elevated levels of PM10 in the vicinity of roads (Lenschow et al., 2001). In Spain field measurements showed that resuspended particles from paved roads had a considerable impact on urban air pollution (Querol et al., 2004b). More recently, the resuspendable amount of particles was experimentally evaluated in the Barcelona area in Spain (Amato et al., 2009a,b; 2010). First model attempts to quantify particle emissions resulting from abrasion of vehicle components and road surface were presented by Rauterberg-Wulff (2000); LUA (2000); Venkatram (2000) following a preliminary formulation by US-EPA (1997). In the present work, HERMES model quantifies particle emissions resulting from abrasion of vehicle components and road surface is based on emission factor calculated by the European study developed by Düring et al. (2002).

The Dust REgional Atmospheric Model (BSC-DREAM8b) was designed to simulate and predict the atmospheric cycle of mineral dust (Nickovic et al., 2001; Pérez et al., 2006a,b). The domain considered in this study comprises northern Africa, the Mediterranean basin and Europe. BSC-DREAM8b is fully embedded within the NCEP/Eta meteorological driver (Janjic, 1994). It simulates the long-range transport of mineral dust at a $0.3^\circ \times 0.3^\circ$ resolution using 24 vertical layers extending up to 15 km in altitude on an hourly basis. The aerosol description contains 8 bins to allow a fine description of dust aerosols. Dust-radiation interactions are calculated online. An offline coupling is applied to the calculated concentrations of particulate matter from CMAQ (Jiménez-Guerrero et al., 2008).

The simulation consists of 366 daily runs constituting the year 2004. The first 12 hours of each daily meteorological runs are treated as cold start, and the next 23 hours are provided to the chemical transport model via the Meteorology-Chemistry Interface Process from CMAQ (MCIP).

2.2 Air Quality Network

In order to evaluate the performances of the CALIOPE system at ground level over Spain, the hourly data from RedESP Spanish network of air quality monitoring stations were selected. The RedESP network comprises a relatively dense geographical coverage of the Spanish territory. The RedESP observational data provided by CEAM were subject to a preliminary quality control to exclude erroneous values. Then, all stations with a temporal coverage below 85% of the entire year 2004 were filtered out. The RedESP stations are characterized the type of zone (urban, suburban and rural) and the dominant emission source (traffic, industrial, and background) based on the proposition by

Garber et al. (2002). Characteristics, location and measured pollutants of the RedESP stations are presented in Tab. 1 and Fig. 2. In summary, a total of 68 measuring stations were used for NO₂, 45 for SO₂, 82 for O₃, and 44 for PM₁₀, respectively.

2.3 Statistical Indicators

A variety of statistical parameters may be used to quantify how well CALIOPE system fits the observation (Denby et al., 2010). In particular, specific metrics were proposed depending on the pollutants (US-EPA, 1984, 1991; Cox and Tikvart, 1990; Weil et al., 1992; Chang and Hanna, 2004; Boylan and Russell, 2006).

Common statistical metrics used by the modeling community include the mean observed and modeled observed, the correlation coefficient (r), the root mean square error (RMSE) and the mean bias (MB). Additionally, the mean normalized bias and gross errors, MNBE and MNGE respectively, considering all modeled/observed pairs of values are also useful parameters. For particulate matter, Boylan and Russell (2006) rather suggested the consideration of the Mean Fractional Bias (MFB) and the Mean Fractional Error (MFE) parameters since they are symmetric metrics, bounding the maximum bias and error.

The US-EPA suggested several performance criteria for simulated O₃, such as MNBE $\leq \pm 15\%$ and MNGE $\leq 35\%$ (US-EPA, 1991, 2007) whereas the EC proposes a modeling quality objective given as a relative uncertainty (%): 50% and 30% for PM₁₀/PM₂₅/O₃ annual average and NO₂/SO₂ annual average, respectively (European Commission, 2008). However, the interpretation of the term model uncertainty remains unclear (Denby et al., 2010). Therefore, the latter criteria will not be further commented in this study. For particulate matter, Boylan and Russell (2006) proposed that the model performance criterion would be met when both MFE $\leq 75\%$ and MFB $\leq \pm 60\%$, respectively, and the model performance goal would be met when MFE and MFB are less than or equal to 50% and $\pm 30\%$, respectively.

The annual mean model-to-data statistics RMSE, correlation coefficient, MNBE, MNGE, MFB and MFE were selected for the present study. According to the recommendations of the US-EPA a cut-off value of 80 $\mu\text{g m}^{-3}$ was applied to O₃ statistics before compilation (US-EPA, 1991; Russell and Dennis, 2000). However, correlation coefficients for O₃ are calculated without cut-off value in order to test the capability of the model to reproduce the variation of O₃ concentrations.

3. Results and discussions

First, this section shows a model evaluation through statistical and dynamical performances. Furthermore, a general description of the annual mean distribution of each pollutant is provided to determine each pattern throughout Spain. Note that statistics are calculated for hourly averages of NO₂, O₃, SO₂, and PM₁₀. In the case of O₃, the daily peak of hourly O₃ is also computed as it is one of the most important parameters to be considered. It is important to remark that neither correction factors nor any adjusting model parameterization were applied to the model output or the original model codes.

3.1 Nitrogen Dioxide

The NO₂ measurement dataset comprises a relatively equal distribution of station types with 21 urban, 22 suburban and 25 rural stations, respectively. Fig. 3a represents the measured (marked black line) and modeled (red line) time series of the hourly mean NO₂ at the 68 measuring stations. The general modeled dynamics is well captured with a clear signal of the main winter pollution events. However, mean levels of NO₂ are persistently underestimated (MB = -12.3 µg m⁻³, not shown).

The statistics compiled in Table 2 show highest mean RMSE values at urban stations (33.6 µg m⁻³) and lowest values for rural stations (7.6 µg m⁻³). This characteristic is not surprising, since urban stations are more likely to be influenced by high, very local emission sources from urban activities which remain difficult to be captured by models. Both MFB and MFE metrics show relatively constant values among the station types, suggesting that the model error for NO₂ is proportional to the normalized observed value. Overall, however, the modeled daily and monthly variations of NO₂ are in good agreement with observations, although a reduced magnitude of the variability is noted. Among the best model behaviours reported, the majority corresponds to either rural stations influenced by background emissions (mean RMSE = 6.3 µg m⁻³ compared to 7.6 µg m⁻³ for all rural stations) or urban stations located in very large (and well characterized) cities such as Madrid or Barcelona (MFB = -46.4% compared to -97.7% for all urban stations). In general, measurements at suburban or urban stations from small- to medium-size cities were simulated with less accuracy. From the 68 stations measuring NO₂, 13 (19%) were not represented correctly by the model. Most of these stations are placed in small cities and are often located in the vicinity of isolated roads or highways (e.g., Acueducto, Estación, Roger Flor, Verge, Table 1). We attribute such behavior to the incomplete characterization of emissions from small cities and to the influence of the model resolution on sub-grid emission sources. The latter, also known as sub-grid variability, is a well-known issue affecting the results of model-observation comparisons (e.g., Ching et al., 2006). Also, NO₂ concentrations in background areas were found to be systematically underestimated. This trend is supported by the lack of biomass burning (Ortiz de Zárate et al., 2005), biogenic soil emissions (Slemr and Seiler, 1984) and natural NO_x production such as lightnings which are currently not treated in the CALIOPE model system (Smith and Mueller, 2010). In addition, biogenic emissions from vegetated and agricultural areas (SNAP10 sector) in HERMES may need further revision.

Fig. 4a displays the annual average modeled levels of NO₂ over Spain. High concentrations of NO₂ within the PBL are directly related to anthropogenic NO_x emission. Baldasano et al. (2008a) estimated that the largest NO_x emission sources come from combustion in energy and transformation industries (41% of NO_x total emission) followed by road transport (37% of NO_x total emission).

The urban plumes from Madrid and Barcelona metropolitan areas reach the highest NO₂ concentrations (~ 25-40 µg m⁻³). In both regions, on-road traffic constitutes the main source of primary pollutants in the region (Gonçalves et al., 2009). In Madrid the NO₂ dispersion follows a south-western direction conditioned by the barrier of Central System (located in the north-western area, 2500 m height) and the canalization of Tajo valley (located in the southern part).

The urban plume reaches the highest concentration at the urban nuclei ($\sim 40 \mu\text{g m}^{-3}$), moving towards Toledo (south) and reaching Guadalajara (east) in a lesser extent. A different NO_2 pattern is observed in Barcelona area. The NO_2 dispersion presents a perpendicular flow to the coast dominated by the north-western winds. The very complex coastal terrain induces mesoscale phenomena which control the superficial wind flows. Sea-breezes and mountain valley winds contribute to the accumulation and recirculation of air masses. The littoral mountain chain (1000 - 1500m height) acts as a barrier, recirculating NO_2 towards the Mediterranean Sea, and also river valleys channel the NO_2 flow.

The densely industrialized area of Tarragona and Castellón and the urban area of Valencia, they all located along the Mediterranean coast, present significant levels of NO_2 affected also by mesoscale phenomena dominated by sea-breezes which determinate NO_2 flow perpendicular to the coast. In the northern Spain, the urban and industrialized area of Bilbao present significant NO_2 levels ($\sim 25 \mu\text{g m}^{-3}$) dispersed along an estuary that runs almost 16 km from the center of the city to the sea and is aligned in an SE-NW direction.

In the north-eastern Spain the NO_2 contribution from power plants emission is bigger than the urban contribution, where NO_2 annual mean concentration reaches $\sim 7\text{-}15 \mu\text{g m}^{-3}$ in the ground level.

Due to the high disaggregation and the specifically detailed emissions implemented in the HERMES model, the impact of principal highways is noticeable, (e.g., Madrid-Sevilla, Barcelona-Bilbao, the A-7 Mediterranean highway) where annual mean values range from 3 to $7 \mu\text{g m}^{-3}$. Background regions, unaffected by emissions rather have concentrations below $3 \mu\text{g m}^{-3}$.

The major shipping route originating from the northern Atlantic and the British Channel, passing along Portugal coast, through the Strait of Gibraltar heading and toward northern Africa and the Suez Canal is shown to have a notable impact on NO_2 levels. Concentrations of NO_2 range from $\sim 5 \mu\text{g m}^{-3}$, near the coastlines of Portugal and Gulf of Cadiz, to $\sim 12 \mu\text{g m}^{-3}$, over the Alboran Sea. This difference is accentuated by the distinct Atlantic-Mediterranean regimes of Spain. Meanwhile in the Mediterranean dynamics in summer is characterized by re-circulation and accumulation of pollutant, a strong dynamically compensated anticyclonic inversion dominates the Spanish Atlantic coast and the west of Portugal (Millán et al., 1997). In the Strait of Gibraltar high NO_2 concentration are estimated ($\sim 30 \mu\text{g m}^{-3}$) where two contributions are combined, the maritime traffic and the industrial processes and electric generation developed in the Algeciras area. The complex topography of the Strait induces the NO_2 dispersion aligned in a west to east direction, with generalized strong east wind (Millán et al., 2002b).

3.2 Ozone

This study comprises a total of 82 RedESP stations measuring O_3 throughout Spain for the year 2004. 24 stations are located in urban areas, 25 in suburban zones and 33 in rural areas, respectively. Modeled and measured time series and scatter plot are presented in Fig. 5 with the corresponding statistics in Tab. 3. Time series for O_3 daily peak (Fig. 5a) show that the O_3 chemistry is best represented in summer. In the high photolytical season, the mean variability and high peaks are generally well reproduced. The modeled variability in winter months is characterized by difficulties to capture the mean trend due to

inaccurate description of cross-tropopause exchanges in CMAQ (Pay et al., 2010). However, the discussion of the evaluation will mainly focus on the high O₃ season (from April to September).

Statistical parameters in hourly basis consistently show better results for stations located in urban areas, followed by suburban and rural areas. The correlation coefficient at all urban stations reaches a maximum of 0.60 with values per station ranging from 0.35 to 0.75. Most of stations display values of MNGE and MNBE lying within the acceptable range defined by the USEPA (Fig. 6c and d, respectively) with low values for MFB and MFE metrics. Table 3 and Fig. 6a also displays the statistics for O₃ daily peaks. Rural areas are characterized by a general underestimation of O₃ daily peaks ($\sim 7 \mu\text{g m}^{-3}$) while peak concentrations at urban stations are rather overestimated ($8.4 \mu\text{g m}^{-3}$) (Fig. 6b). High correlations are noted for each type of station. In summary the model system used in this study performs well with respect to the simulation of high O₃ concentrations over Spain. However, an overestimation of nocturnal values is depicted with recurrent low daily variations due to uncertainties in the modeled nocturnal NO_x cycle, which is a common feature in chemical transport models.

Stations influenced by traffic emissions (i.e. high NO_x emissions) are better characterized with a more pronounced daily O₃ variability. To complement such finding, Fig. 7, representing the O₃ model-to-observation bias as a function of the modeled NO₂ concentrations for all the 68 stations measuring both NO₂ and O₃, is proposed in order to evaluate the performances of the model with respect to the NO_x/O₃ chemistry.

While a deviation from the O₃ bias is mainly constrained by the lateral chemical boundary conditions, the width of the plotted dataset is controlled by the chemical mechanism implemented in the model. This figure clearly shows that the highest uncertainties in the reproduction of O₃ levels are related to NO₂-limited regime. Under this regime, corresponding to background conditions, the O₃ bias is slightly shifted to the right, meaning that the modeled O₃ tends to overestimate observed values, specifically during nighttime (also see mean observed and modeled values for rural stations in Tab. 3). As a contrary, the width of O₃ model-to-observation biases decreases with increasing modeled NO₂. Such behavior reflects the better representation of the NO_x/O₃ chemistry under non-limited-NO₂ regimes, but it also shows that the chemistry under higher-NO₂ regime has a reduced dependency to the lateral chemical conditions of the model (no shift on the X-axis). As an example, data from Sierra Norte (Rural Background, light grey triangles) and Recoletos (Urban Traffic, dark grey squares) are overlaid on the figure. The O₃ bias at Sierra Norte displays a wide variability related to low modeled NO₂ whereas the bias for Recoletos markedly diminishes with increasing modeled NO₂. Such description confirms the higher performances of the model for urban stations than for rural stations. This behavior highlights the need to better characterize the emission inventory for background areas (see discussion in Sect. 3.1). The curve interpolating the average O₃ bias in vertical also confirms the higher bias values under low NO₂ regime (maximum bias O₃ $\sim 22 \mu\text{g m}^{-3}$ for $[\text{NO}_2]_{\text{model}} = 15 \mu\text{g m}^{-3}$), while it remains significantly lower for NO₂ modeled concentration above $60 \mu\text{g m}^{-3}$.

The annual mean distribution of O₃ over the IP is presented in Fig. 4b. Highest mean concentrations are located in the open Mediterranean Sea (up to $90 \mu\text{g m}^{-3}$) and the Spanish Mediterranean coast ($\sim 80 \mu\text{g m}^{-3}$). Such concentrations are favoured by the prevailing intense photochemistry in the

region (EEA, 2005; Vautard et al., 2005b), the local formation and transport (Lelieveld et al., 2002; Gerasopoulos et al., 2005; Cristofanelli and Bonasoni, 2009), the persistent subsidence over the region (Millán, 2002a) and the low O₃ depletion over sea. The Spanish oceanic region in the north and north-western Spain, characterized by high frequency of precipitation presents lower O₃ levels than the Spanish arid and mediterranean regions. The wet deposition of O₃ is an important sink in the oceanic regions, meanwhile local generation and transport are the processes which contribute to O₃ levels in arid and Mediterranean regions.

The Fig. 4b also highlights significant levels over the major Spanish mountain ranges such as the Pyrenean chain, the Baetic Cordillera (southeastern Spain) or the Sierra Norte (laying north of Madrid in a west-to-northeast direction), reflecting the O₃ vertical gradient in the atmosphere.

O₃ is found lowest ($\sim 50 \mu\text{g m}^{-3}$) in either regions of low precursor emissions (northern and southern plateaus) or in areas affected by large NO-to-NO₂ concentration ratios (e.g., zones of intense on-road and ship traffic). Reactions involving nitrogen oxides are wellknown key reactions controlling the amount of O₃ in the troposphere (Fishman and Crutzen, 1978). In this chemical regime reactions between NO₂ and O₃ prevail, leading to low levels of O₃. These areas comprise the major Spanish metropolitan cities (i.e., Madrid, Barcelona, Valencia, Sevilla), highways of high traffic flow (like NO₂, see Sect. 3.1) and the major shipping routes in the Mediterranean Sea.

3.3 Sulfur Dioxide

From a total of 45 stations measuring SO₂, 13 are located in urban areas, 14 in suburban and 18 in rural areas, respectively. In Spain, SO₂ is mainly produced by power generating and transformation industries. Indeed, Linares and Romero (2000) reported that electricity generation contributes 66% to the total SO₂ emitted in Spain. These very localized industries generate large plumes of high-SO₂ content affecting the air quality on a local to national scale. Modeling SO₂ for air quality purposes is a complex issue, since the accuracy in the meteorological patterns is crucial for the determination of plume dynamics. Also, the variability on the sub-grid scale must be considered when comparing model results with measured data. The mean hourly SO₂ variability and levels are very well captured by the modeling system (Fig. 3b). Episodic extreme values are underestimated in general, although the model is capable of reproducing the trend. Mean biases are low (from -3.1 for urban to $0.6 \mu\text{g m}^{-3}$ for suburban stations). Due to the frequently episodic character of high SO₂ events and their dependency to meteorology correlation coefficients are rather low ($r=0.14$ for urban/suburban stations; 0.28 for rural stations). Highest correlations were obtained for background stations ($r= 0.34$). MFB values show good performance comparing with the other primary pollutants ($-47.1\% < \text{MFB} < -23.8\%$) but MFE values highlight the need to further improve the modeled SO₂ physico-chemistry. Among the 45 stations measuring SO₂ in the Peninsula, the model-to-data comparison was distinctly unsatisfactory for three locations (7% of the total). Two of these locations were found in the same grid cell as large power plants (Abanto and Grao). A third station ("Salamanca2" in the city of Salamanca) displays high SO₂ measured concentrations which are strongly underestimated by the model. Such behavior may be explained by emission sources unaccounted by the

model system or by the erroneous coordinates of the instrument.

In Spain, Baldasano et al. (2008a) reported that combustion in energy and transformation industries contributes 83% to the total SO₂ emitted in Spain. In this framework, the SO₂ is emitted mainly from large isolated point sources, instantaneously mixed in high layers in the atmosphere and transported and dispersed following the plume dynamic. The mean chemical distribution of SO₂ over the IP, shown in Fig. 4c, is characterized by two major patterns. First, the Spanish territory is marked by various emission hot-spots often reaching air concentrations above 15 µg m⁻³. These localized sources originate mainly from power plants and refineries.

Northern Spain suffers substantial SO₂ mean annual levels of up to ~ 10 µg m⁻³ due to the presence of geographically-close power plants and refineries in the area of Galicia, Ponferrada, Asturias and Bilbao. SO₂ reaches maximum levels (~ 50 µg m⁻³) near the two refineries in Bilbao and La Coruña. The SO₂ dispersion pattern in north-western Spain is significantly dominated by the northern and north-western winds that transport SO₂ inland. Eastern Spain is mostly affected by a thermo-electrical power plant from Teruel (Aragón region), the pattern is dominated by the canalization of the Ebro valley towards the Mediterranean sea. The southern Spanish plateau displays high SO₂ levels around Puertollano (Castilla-La Mancha region) due to the presence of a refinery and two power plants.

In the urban areas the SO₂ dispersive pattern remains ~ 6 µg m⁻³; in Madrid and Barcelona cities the levels of SO₂ are sum of two contributions, the on-road traffic and the cogeneration plants. Minimum concentrations from unpolluted areas display mean values near 0.5-2 µg m⁻³.

The second pattern dissociated from this figure is the shipping route from the Atlantic, through the Strait of Gibraltar, toward the major Mediterranean harbours. Ship emissions are large contributors to the total SO_x concentrations along the main ship tracks due to fuel combustion of high sulfur content (Corbett and Fischbeck, 1997; Corbett and Koehler, 2003), although ship emission abatement strategies are under current application (Internacional Maritime Organization and Marine Environment Protection Committee, 2001). These emissions from maritime zones lead to coastal mean SO₂ concentrations from 2 to 8 µg m⁻³ on annual average, with a maximum of 12-18 µg m⁻³ in the narrow Gibraltar regions with a dispersion pattern dominated by western winds. The SO₂ contribution of shipping route in this area is combined with the contribution from one large refinery, industrial processes, and electric generation carried out in the Gibraltar bay.

3.4 Particulate matter

A total of 44 RedESP stations measured particulate matter concentrations over the IP and the Balearic Islands for the year 2004. 12 stations were located in rural areas, 17 in suburban and 15 in urban areas, respectively. Among these 44 stations, the model represented the PM concentrations fairly well at 17 locations (nearly 40% of the total). These locations were mostly background rural. In these areas mean concentrations are often low with episodic high concentration peaks. The implementation of the Sahara desert dust contribution from the BSC-DREAM8b model is responsible for the satisfactory representation of such concentration peaks. The evaluation of the modeling system highlighted

less accurate modeled levels at suburban and urban locations mostly influenced by background emissions. Model-to-data comparisons in urbanized areas of industrial or traffic emissions showed lowest accuracy. We attribute such behavior to the defective characterization of emission sources in areas of intense human activity.

Fig. 3c clearly highlights two distinct aspects of the model in the representation of PM₁₀ concentrations at all available stations. Modeled concentrations were persistently underestimated throughout the year 2004. This underestimation is a common feature of most of the current regional models (Pay et al., 2010). The mean annual bias amounts to $-21.8 \mu\text{g m}^{-3}$ with an annual RMSE value of $33.4 \mu\text{g m}^{-3}$. On the other hand, the general PM₁₀ dynamics are well captured, with the major events correctly modeled and synchronized with measured amounts. The mean correlation for all stations amounts to 0.38 with higher correlations at rural stations ($r = 0.43$, ranging from 0.28 to 0.58 per station). Due to the important underestimation of the model concentrations, MFB and MFE values are undoubtedly ranging above the criteria for acceptable model performances proposed by Boylan and Russell (2006).

Fig. 4d shows the annual average pattern of natural and anthropogenic PM₁₀ over the IP for 2004. Concentrations present a large variability across Spain depending on emission sources, climate and reactivity/stability of particulate species (see Querol et al., 2001, 2003, 2004a, 2008; Rodríguez et al., 2002; Viana et al., 2005). The spatial distribution of PM₁₀ annual mean modelled levels shows that particle concentrations reach high values ($\sim 15 \mu\text{g m}^{-3}$) in large cities like Madrid, Barcelona, Valencia, and Bilbao there is an important contribution of exhaust and non-exhaust emissions from road transport in urban areas.

Marine aerosols contribute nearly 3 and $5 \mu\text{g m}^{-3}$ to the annual mean PM₁₀ concentration over the Mediterranean and Atlantic coasts, respectively (not shown). This difference in concentration reflects the higher wind speeds and fetch distances in the Atlantic than in the Mediterranean Basin leading to more transport of sea salt aerosols from the Atlantic open ocean to the coasts. The contribution of marine aerosols to PM₁₀ annual concentrations over the open ocean ranges from 6 (Mediterranean Basin) to $9 \mu\text{g m}^{-3}$ (Atlantic) which is consistent with model data from Manders et al. (2010).

In the north, the industrial areas in Castellón dominated by ceramic industry, present high levels of PM₁₀, dispersed along a perpendicular axis to the coast. Mediterranean coast presents PM₁₀ dispersion pattern influenced sea-breezes combined with upslope winds to create recirculations along the coast and within the western Mediterranean basin. In summer the higher temperatures and solar radiation lead to the formation of secondary aerosols contributing to the levels of particulate matter. The Ebro valley acts by channelling particulate matter flow inland. Meanwhile in the northern coastal Spain the Atlantic winds dominate the transport of particulate matter inland.

Large sources of SO₂ located in wet Spain region, in the north, (Fig. 4c) do not contribute efficiently to the secondary inorganic aerosol since high dispersion and removal by wet deposition are important processes in this region (not shown). In the southern part of Spain, African dust outbreaks contribute significantly to the aerosol loadings, ranging from 10 to $20 \mu\text{g m}^{-3}$. The largest annual mean contribution of desert dust coincides with the Sierra Nevada mountain range with values reaching up to $30 \mu\text{g m}^{-3}$. Such concentrations are

the consequences of (1) the mountain range location within the main zone of dust deposition (70% of dust export is deposited within the first 2000 km, Jaenicke and Schütz, 1978) and (2) the existence of several peaks within the mountain range 3000 m above sea level (asl) which corresponds to the altitude range for Saharan dust transport (between 1500 and 4000 m asl, Talbot et al., 1986; Olmo et al., 2008).

4. Exceedances of ozone during summertime

This section analyses the O₃ exceedances during the high O₃ season (from April to September) when O₃ concentrations present peaks which frequently exceeded 120 µg m⁻³, reaching still 200 µg m⁻³. The target value set in the European regulation is 120 µg m⁻³, not to be exceeded on more than 25 days per calendar year averaged over three years (averaging as the maximum daily eight-hour mean, European Commission, 2008). Fig. 8 shows the number of days exceeding the concentration value of 120 µg m⁻³ for the 8-hr maximum O₃ concentration and the VOCs/NO_x ratio over the land domain (Fig. 8a) and over the entire domain, including the ocean (Fig. 8b). The VOCs/NO_x ratio is calculated as hourly average and is represented in logarithm scale, since the ratio ranges from 1 to 10⁶.

There is an overlap among ratios and number of days with exceedances. The number of exceedances is higher than 45 days where VOCs/NO_x ratio is between 3 and 4.5, approximately. Such situation correspond to zones downwind main NO_x emission sources (see annual mean concentration of NO₂ in Fig. 4a) from the two largest Spanish cities (Madrid and Barcelona, see locations in Fig. 8) and industrial areas along the eastern Spanish Mediterranean coast (Tarragona, Valencia and Castellón; see locations in Fig. 8). Dynamics of pollutant during summer and primary emission sources along the eastern coast and the central plateau of the IP determinate the location of the calculated exceedances. Several studies performed over the western Mediterranean basin (e.g. Gangoiti et al., 2001; Jiménez and Baldasano, 2004; Stein et al., 2005; Jiménez et al., 2006; Jiménez-Guerrero et al., 2008b; Gonçalves et al., 2009) are in agreement with our findings. Along the coast the sea-breezes and mountain-valley winds contribute to the accumulation and recirculation of aged air masses and O₃ aloft. Besides, over the central plateau flows are dominated by the development of the IP Thermal Low (ITL). Several deep convective cells coupled with the ITL inject aged pollutant for the Madrid area and those transported previously from coastal area. On the other hand, the number of exceedances is less than 30 days for VOCs/NO_x ratio higher than 4.75, that regime, represented in white color in Fig. 8, covers the northern and southern Spanish plateaus, where there is no high density of anthropogenic emissions. Note that a quarter of the IP presents more than 30 days exceeding the value of 120 µg m⁻³ for the 8-hr maximum O₃ concentration.

In general, there is a significant anti-correlation ($r=-0.71$) between O₃ exceedances and the VOCs/NO_x ratio for the entire domain when only the inland O₃ formation is considered (Fig. 8a). For high ratios, there is a NO_x limitation regime, and no O₃ exceedances are detected because of there is not enough NO_x available. However, when we calculate the aforementioned correlation over the entire domain, including the ocean (Fig. 8b), the anti-correlation slightly

decreases ($r=-0.63$) as a result of two different behaviors. First, the Strait of Gibraltar region presents the lowest VOCs/NO_x ratio (equal to 3) and no exceedances are detected (see Sect. 3.2). The frequent shipping traffic and the high density of industry in the area generate important NO_x emissions, VOCs concentrations are not high enough to produce O₃, moreover the O₃ loss is high due to NO_x emissions act as O₃ sinks (Marmer et al., 2009). The opposite happens over the western Mediterranean basin which shows the highest VOCs/NO_x ratio (over 5) and many exceeding days (more than 45). As we mentioned before, the complex layout of the coasts and surrounding mountain favors that the Mediterranean Sea acts as a reservoir of aged pollutants. Furthermore in summer the meteorological condition (high pressure, stability, clear sky and high solar radiation intensity) enhance photochemical processes and emissions of biogenic volatile organic compounds to the atmosphere (NO_x limited regime). Not only O₃ formation due to local and regional sources, but also long-range transport of European air toward the Mediterranean basin (Lelieveld et al., 2002) could be important causes of the O₃ exceedances of the limit value. Furthermore dry deposition over open ocean remains near zero (not shown here). All together contribute to increase levels of O₃ (lifetime typically of few weeks in summer, Seinfeld and Pandis, 1998).

5. Conclusions

This work presents the evaluation and the assessment of the CALIOPE air quality forecasting system (namely WRF-ARW/HERMES/CMAQ/BSC-DREAM8b) for a full-year simulation for 2004 over Spain. CALIOPE was applied with high resolution (4 km x 4 km, 1 hr) using the HERMES emission model specifically developed for Spain. The evaluation of the modeling results for gas-phase pollutants (O₃, NO₂ and SO₂) and particulate matter (PM₁₀) on an hourly basis showed a strong dependency of the performance of the model on the type of zone (urban, suburban and rural) and the dominant emission sources (traffic, industrial, and background). For NO₂ the best model behavior corresponds to both background rural stations and urban stations located in very large cities such as Madrid or Barcelona. With respect to O₃, stations influenced by traffic emissions (i.e. high NO_x emissions) are better characterized with a more pronounced daily variability. NO_x/O₃ chemistry is better represented under non-limited-NO₂ regimes. For each station category, annual O₃ (hourly and peaks) statistics meet the range defined by the USEPA and European regulation for an acceptable performance of the model. Results show that a quarter of the Iberian Peninsula is affected by more than 30 days exceeding the value of 120 µg m⁻³ for the 8-hr maximum O₃ concentration.

The general spatial patterns and temporal characteristics simulated by CALIOPE for gas-phase pollutants and particulate matter are consistent with other studies and surveys. SO₂ is mainly produced from isolated point sources (power generation and transformation industries) which generate large plumes of high SO₂ concentration affecting the air quality on a local to national scale where the meteorological pattern is crucial, whereas NO₂ concentration in ground level are dominated mainly by traffic emissions, which are subjected to a much stronger temporal variation than the SO₂ emissions.

NO₂ mean levels are persistently underestimated (MB = -12.3 µg m⁻³).

Highest errors are found in urban stations which are likely influenced by high, very local emission sources from urban activities which remain difficult to capture by models. NO₂ stations located in small cities were not represented correctly by the model. We attribute such behavior to the incomplete characterization of emissions from small cities and to the influence of the model resolution on sub-grid emission sources. Modeled PM10 concentrations were persistently underestimated at suburban and urban locations mostly influenced by background emissions, a common feature of most of the current regional models.

Despite the accurate performance of the modeling system, several aspects are now under further research in the framework of the CALIOPE project. Wind-blown dust should be taken into account since such source contributes to the underestimation of the total concentration of PM10, especially in dry and arid regions such Spain. Biomass burning, biogenic soil emissions and natural NO_x are currently not treated in the CALIOPE model system, and could contribute to the NO₂ underestimation. In addition, ammonia emission and particulate matter from vegetated and agricultural areas in HERMES are under a continuous improvement. Last, a new version of CMAQ is being implemented in the MareNostrum supercomputing (CMAQv4.7) featuring a new aerosol module which contains substantial scientific improvements over the aerosol modules released in version 4.5, especially devoted to improve secondary organic aerosol formation.

The present analysis demonstrates that the high spatial resolution (4 km x 4 km) applied in the CALIOPE forecasting system correctly address the air pollution behavior in (1) urban/industrial areas with a pervasive influence of anthropogenic emissions on a local scale, and (2) areas with very complex terrains and meteorology like southern Europe. Therefore, the system has been implemented and evaluated operationally and air quality forecasts can be found in <http://www.bsc.es/caliope>.

6. Acknowledgements

The authors wish to thank the CEAM, CIEMAT and CSIC-IJA centers for their collaboration in the project. Also, thanks to S. Basart and C. Pérez for providing the BSC-DREAM8b outputs and L. González for their work related to the CALIOPE system. This work is funded by the CALIOPE project of the Spanish Ministry of the Environment (441/2006/3-12.1, A357/2007/2-12.1, 157/PC08/3-12.0). The Spanish Ministry of Science and Innovation is also thanked for the Formación de Personal Investigador (FPI) doctoral fellowship held by María Teresa Pay (CGL2006-08903). All simulations were performed on the MareNostrum supercomputer hosted by the Barcelona Supercomputing Center.

References

Amann, M., Bertok, I., Cofala, J., Gyarmas, F., Heyes, C., Klimont, Z., Schöpp, W., Winiwarter, W., 2004. Baseline Scenarios for the Clean Air for Europe (CAFE) Programme. Technical Report. European Commission, DG Environment, Dir. C Environment and Health.

Amato, F., Pandolfi, M., Escrig, A., Querol, X., Alastuey, A., Pey, J., Pérez, N., Hopke, P.K., 2009a. Quantifying road dust resuspension in urban environment by multilinear engine: A comparison with pmf2. *Atmos. Environ.* 43, 2770-2780.

Amato, F., Pandolfi, M., Viana, M., Querol, X., Alastuey, A., Moreno, T., 2009b. Spatial and chemical patterns of PM₁₀ in road dust deposited in urban environment. *Atmos. Environ.* 43, 1650-1659.

Amato, F., Nava, S., Lucarelli, F., Querol, X., Alastuey, A., Baldasano, J.M., Pandolfi, M., 2010. A comprehensive assessment of PM emissions from paved roads: Real-world Emission Factors and intense street cleaning trials. *Sci. Tot. Env.* 408, 4309-4318.

Baldasano, J.M., Cremades, L., Soriano, C., 1994. Circulation of air pollutants over the Barcelona geographical area in summer. Proceedings of Sixth European Symposium Physic-Chemical Behavior of Atmospheric Pollutants. Varese (Italy), 18-22 October, 1993. Report EUR 15609/ EN: 474-479.

Baldasano, J.M., Jiménez-Guerrero, P., Jorba, O., Pérez, C., López, E., Güereca, P., Martín, F., Vivanco, M.G., Palomino, I., Querol, X., Pandolfi, M., Sanz, M.J., Diéguez, J.J., 2008a. Caliope: an operational air quality forecasting system for the Iberian Peninsula, Balearic Islands and Canary Islands - first annual evaluation and ongoing developments. *Adv. Sci. Res.* 2, 89-98.

Baldasano, J.M., Güereca, L.P., López, E., Gassó, S., Jiménez-Guerrero, P., 2008b. Development of a high-resolution (1 km x 1 km, 1h) emission model for Spain: The High-Effective Resolution Modelling Emission System (HERMES). *Atmos. Environ.* 42, 7215-7233.

Binkowski, F.S., 1999. Aerosols in models-3 cmaq, in: Byun, D.W., Ching, J.K.S. (Eds.), *Science Algorithms of the EPA Models-3 Community Multiscale Air Quality (CMAQ) Modeling System*, EPA. pp. 10-23.

Binkowski, F.S., Roselle, S.J., 2003. Models-3 community multiscale air quality (cmaq) model aerosol component. 1. model description. *J. Geophys. Res.* 108 (D6), 4183, doi:10.1029/2001JD001409.

Binkowski, F.S., Shankar, U., 1995. The regional particulate model 1. model description and preliminary results. *J. Geophys. Res.* 100 (D12), 26191-26209.

Boylan, J., Russell, A., 2006. Pm and light extinction model performance metrics, goals, and criteria for three-dimensional air quality models. *Atmos. Environ.* 40, 4946-4959.

Brunekreef, B., Holgate, S.T., 2002. Air pollution and health. *Lancet* 360 (9341), 1233-1242, doi:10.1016/S0140-6736(02)11274-8.

Byun, D., Schere, K.L., 2006. Review of the governing equations,

computacional algorithms, and other components of the Models-3 Community Multiscale Air Quality (CMAQ) modeling system. *Appl. Mech. Rev.* 59 (2), 51-77.

Byun, D.W., Ching, J.K.S., 1999. Science algorithms of the EPA Models-3 Community Multiscale Air Quality (CMAQ) modeling system. Atmospheric modeling division, National Exposure Research Laboratory, US Environmental Protection Agency, Research Triangle Park, NC 27711.

Chang, J.C., Hanna, S.R., 2004. Air quality model performance evaluation. *Meteorol. Atmos. Phys.* 87, 167-196.

Ching, J., Herwehe, J., Swall, J., 2006. On joint deterministic grid modeling and sub-grid variability conceptual framework for model evaluation. *Atmos. Environ.* 40, 4935-4945.

Corbett, J.J., Fischbeck, P., 1997. Emissions from ships. *Science* 278 (5339), 823-824, doi:10.1126/science.278.5339.823.

Corbett, J.J., Koehler, H.W., 2003. Updated emissions from ocean shipping. *J. Geophys. Res.* 108 (D20), 4650, doi:10.1029/2003JD003751.

Cox, W.M., Tikvart, J.A., 1990. Statistical procedure for determining the best performing air quality simulation model. *Atmos. Environ.* 24, 2387-2395.

Cristofanelli, P., Bonasoni, P., 2009. Background ozone in the southern Europe and Mediterranean area: Influence of the transport processes. *Env. Poll.* 157, 1399-1406.

Cuvelier, C., Thunis, P., Vautard, R., Amann, M., Bessagnet, B., Bedogni, M., Berkowicz, R., Brandt, J., Brocheton, F., Builtjes, P., Carnavale, C., Coppalle, A., Denby, B., Douros, J., Graf, A., Hellmuth, O., Hodzic, A., Honoré, C., Jonson, J., Kerschbaumer, A., de Leeuw, F., Minguzzi, E., Moussiopoulos, N., Pertot, C., Peuch, V.H., Pirovano, G., Rouil, L., Sauter, F., Schaap, M., Stern, R., Tarrason, L., Vignati, E., Volta, M., White, L., Wind, P., Zuber, A., 2007. Citydelta: A model intercomparison study to explore the impact of reductions in European cities in 2010. *Atmos. Environ.* 41, 189-207.

Denby, B., Larssen, S., Guerreiro, C., Li, L., Douros, J., Moussiopoulos, N., Fragkou, L., Gauss, M., Olesen, H., Miranda, A.I., Georgieva, E., Dilara, P., Lappi, S., Rouil, L., Lükeville, A., Querol, X., Martin, F., Schaap, M., van den Hout, D., Kobe, A., 2009. Guidance on the use of models for the European Air Quality Directive. A working document of the Forum for Air Quality Modelling in Europe FAIRMODE. Technical Report Version 4.2, Editor B. Denby. ETC/ACC report.

Düring, I., Jacob, J., Lohmeyer, A., Lutz, M., Reichenbacher, W., 2002. Estimation of the "non-exhaust pipe" PM₁₀ emissions of streets for practical traffic air pollution modelling, in: 11th Intl. Symposium TRANSPORT and AIR POLLUTION, Graz University of Technology, Institute for Internal Combustion Engines and Thermodynamics. pp. 309-316, vol. 1.

EEA, 2005. Air pollution by ozone in Europe in summer 2004. Technical Report. 3/2005, Copenhagen, Denmark. <http://reports.eea.eu.int>.

EEA, 2009a. Air pollution by ozone across Europe during summer 2008. Technical Report. 2/2009, Copenhagen, Denmark. <http://reports.eea.eu.int>.

EEA, 2009b. Spatial assessment of PM₁₀ and ozone concentrations in Europe (2005). Technical Report. 1/2009, Copenhagen, Denmark. <http://reports.eea.eu.int>.

EEA, 2010. Air pollution by ozone across Europe during summer 2009. Technical Report. 2/2010, Copenhagen, Denmark. <http://reports.eea.eu.int>.

European Commission, 2008. Directive 2008/50/EC of the European Parliament and of the Council of 21 May 2008 on ambient air quality and cleaner air for Europe. Technical Report 2008/50/EC, L152. Off. J. Eur. Comm.

Fishman, J., Crutzen, P., 1978. The origin of ozone in the troposphere. *Nature* 274, 855-858.

Folberth, G., Hauglustaine, D.A., Lathière, J., Brocheton, J., 2006. Interactive chemistry in the laboratoire de météorologie dynamique general circulation model: model description and impact analysis of biogenic hydrocarbons on tropospheric chemistry. *Atmos. Chem. Phys.* 6, 2273-2319.

Gangoiti, G., Millán, M., Salvador, R., Mnatilla, E., 2001. Long-range transport and re-circulation of pollutants in the western Mediterranean during the project regional cycles of air pollution in the west-central Mediterranean area. *Atmos. Environ.* 35, 6267-6276.

Garber, W., Colosio, J., Grittner, S., Larssen, S., Rasse, D., Schneider, J., Housiau, M., 2002. Guidance on the Annexes to Decision 97/101/EC on Exchange of Information as revised by Decision 2001/752/EC. Technical Report. European Commission, DG Environment.

Gerasopoulos, E., Kouvarakis, G., Vrekoussis, M., Kanakidou, M., Mihalopoulos, N., 2005. Ozone variability in the marine boundary layer of the eastern Mediterranean based on 7-year observations. *J. Geophys. Res.* 110, D15309.

Gery, M.W., Whitten, G.Z., Killus, J.P., Dodge, M.C., 1989. A photochemical kinetics mechanism for urban and regional scale computer modeling. *J. Geophys. Res.* 94 (D10), 12925-12956.

Gonçalves, M., Jiménez-Guerrero, P., Baldasano, J., 2009. Contribution of atmospheric processes affecting the dynamics of air pollution in south-western Europe during a typical summertime photochemical episode. *Atmos. Chem. Phys.* 9, 849-864.

Gong, S.L., 2003. A parameterization of sea-salt aerosol source function for sub- and super-micron particles. *J. Geophys. Res.* 17, 1097, doi:10.1029/2003GB002079.

Gryparis, A., Forsberg, B., Katsouyanni, K., Analitis, A., Touloumi, G., Schwartz, J., Samoli, E., Medina, S., Anderson, H.R., Niciu, E.M., Wichmann, H.E., Kriz, B., Kosnik, M., Skorkovsky, J., Vonk, J.M., Dörtbudak, Z., 2004. Acute effects of ozone on mortality from the air pollution and health: A European approach project. *Amer. J. Resp. Crit. Care Med.* 170 (10), 1080-1087.

Hauglustaine, D.A., Hourdin, F., Jourdain, L., Filiberti, M.A., Walters, S., Lamarque, J.F., Holland, E.A., 2004. Interactive chemistry in the laboratoire de meteorologie dynamique general circulation model: Description and background tropospheric chemistry evaluation. *J. Geophys. Res.* D4 (D04314), doi:10.1029/2003JD003,957.

International Maritime Organization and Marine Environment Protection Committee, 2001. Prevention of air pollution from ships-Sulfur monitoring 2000. Technical Report. London.

Jaenicke, R., Schütz, L., 1978. Comprehensive study of physical and chemical properties of the surface aerosols in the Cape Verde islands region. *J. Geophys. Res.* 83 (C7), 3585-3599.

Janjic, Z.I., 1994. The step-mountain ETA coordinate model: Further developments of the convection, viscous sublayer and turbulence closure schemes. *Mon. Weather Rev.* 122, 927-945.

Jiménez, P., Baldasano, J.M., Dabdub, D., 2003. Comparison of photochemical mechanisms for air quality modelling. *Atmos. Environ.* 37 (30), 4179-4194, doi:10.1016/S1352-2310(03)00567-3.

Jiménez, P., Baldasano, J.M., 2004. Ozone response to precursor controls in very complex terrains: Use of photochemical indicators to assess O₃-NO_x-VOC sensitivity in the northeastern Iberian Peninsula. *Journal of Geophysical Research* 109, D20309, doi: 10.1029/2004JD004985.

Jiménez, P., Lelieveld, J., Baldasano, J.M., 2006. Multi-scale modeling of air pollutants dynamics in the northwestern Mediterranean basin during a typical summertime episode. *J. Geophys. Res.* 111, (D18306), 1-21, doi:10.1029/2005JD006516.

Jiménez-Guerrero, P., Jorba, O., Baldasano, J.M., Gassó, S., 2008. The use of a modelling system as a tool for air quality management: Annual high resolution simulations and evaluation. *Sci. Tot. Env.* 390, 323-340.

Jiménez-Guerrero, P., Pérez, C., Jorba, O., Baldasano, J.M., 2008. Contribution of Saharan dust in an integrated air quality system and its on-line assessment. *Geophys. Res. Lett.* 35 (L03814), doi:10.1029/2007GL031580.

Lam, Y.F., Fu, J.S., 2009. A novel downscaling technique for the linkage of global and regional air quality modeling. *Atmos. Chem. Phys.* 9, 9169-9185.

de Leeuw, F., Vixseboxse, E., 2010. Reporting on ambient air quality assessment - Preliminary results for 2008. Technical Report. The European Topic Centre on Air and Climate Change (ETC/ACC) Technical Paper 2009/10.

Lelieveld, J., Berresheim, H., Borrmann, S., Crutzen, P.J., Dentener, F.J., Fischer, H., Feichter, J., Flatau, P.J., Heland, J., Holzinger, R., Korrmann, R., Lawrence, M.G., Levin, Z., Markowicz, K.M., Mihalopoulos, N., Minikin, A., Ramanathan, V., de Reus, M., Roelofs, G.J., Scheeren, H.A., Sciare, J., Schlager, H., Schultz, M., Siegmund, P., Steil, B., Stephanou, E.G., Stier, P., Traub, M., Warneke, C., Williams, J., Ziereis, H., 2002. Global air pollution crossroads over the Mediterranean. *Science* 298, 794-799.

Lenschow, P., Abraham, H.J., Kutzner, K., Lutz, M., Preuß, J.D., Reichenbacher, W., 2001. Some ideas about the sources of PM₁₀. *Atmos. Environ.* 35, Supplement No. 1, S23.

Linares, P., Romero, C., 2000. A multiple criteria decision making approach for electricity planning in Spain: economic versus environmental objectives. *J. Oper. Res. Soc.* 51 (6), 736-743.

LUA, 2000. Vorgehensweise bei der Schwebstaubimmissionsberechnung nach Richtlinie 1999/30/EG. Technical Report. Landesumweltamt Brandenburg, Entwurf des Referats I3 vom 21.12.2000.

Manders, A., Schaap, M., Querol, X., Albert, M.F.M.A., Vercauteren, J., Kuhlbusch, T.A.J., Hoogerbrugge, R., 2010. Sea salt concentrations across the European continent. *Atmos. Environ.*, in press.

Marmer, E., Dentener, F., Aardenne, J., Cavalli, F., Vignati, E., Velchev, K., Hjorth, J., Boersma, F., Vinken, G., Mihalopoulos, N., Raes, F., 2009. What can we learn about ship emission inventories from measurements of air pollutants over the Mediterranean Sea? *Atmos. Chem. Phys. Discuss.* 9, 7155-7211.

Menut, L., Bessagnet, B., 2010. Atmospheric composition forecasting in Europe. *Annals Geoph.* 28, 61-74.

Michalakes, J., Dudhia, J., Gill, D., Henderson, T., Klemp, J., Skamarock, W., Wang, W., 2004. The weather research and forecast model: Software architecture and performance, in: Mozdzyński, E.G. (Ed.), To appear in proceeding of the Eleventh ECMWF Workshop on the Use of High Performance Computing in Meteorology, 2529 October 2004, Reading, U.K.. p. 117-124.

Millán, M.M., Salvador, R., Mantilla, E., 1997. Photooxidant dynamics in the Mediterranean Basin in Summer: Results from European Research Projects. *J. Geophys. Res.* 102(D7), 8811-8823.

Millán, M.M., 2002a. Ozone Dynamics in the Mediterranean Basin, A

collection of scientific papers resulting from the MECAPIP, RECAPMA and SECAP Projects. Technical Report. European Commission and CEAM.

Millán, M.M., Sanz, M.J., Salvador, R., Mantilla, E., 2002b. Atmospheric dynamics and ozone cycles related to nitrogen deposition in the western Mediterranean. *Energy Policy* 118, 167-186.

Nenes, A., Pilinis, C., Pandis, S.N., 1998. ISORROPIA: A new thermodynamic equilibrium model for multiphase multicomponent inorganic aerosols. *Aquatic Geochemistry* 4 (1), 123-152, doi:10.1023/A:1009604003981.

Nickovic, S., Kallos, G., Papadopoulos, A., Kakaliagou, O., 2001. A model for prediction of desert dust cycle in the atmosphere. *J. Geophys. Res.* 106 (D16), 18113-18129, doi:10.1029/2000JD900794.

Olmo, F.J., Quitantes, A., Lara, V., Lyamani, H., Alados-Arboledas, L., 2008. Aerosol optical properties assessed by an inversion method using the solar principal plane for non-spherical particles. *J. Quant. Spectrosc. Radiat. Transfer* 109, 1504-1516.

Ortiz de Zárate, I., Ezcurra, A., Lacaux, J.P., Dinh, P.V., de Argandoña, J.D., 2005. Pollution by cereal waste burning in Spain. *Atmos. Res.* 73 (1-2), 161-170, doi:10.1016/j.atmosres.2004.07.006.

Pay, M.T., Piot, M., Jorba, O., Basart, S., Gassó, S., Jiménez-Guerrero, P., Gonçalves, M., Dabdub, D., Baldasano, J.M., 2010. A full year evaluation of the CALIOPE-EU air quality system in Europe for 2004: a model study. *Atmos. Environ.*, doi:10.1016/j.atmosenv.2010.050140.

Pénard-Morand, C., Charpi, D., Raheison, C., Kopferschmitt, C., Caillaud, D., Lavaud, F., Annesi-Maesano, I., 2005. Long-term exposure to background air pollution related to respiratory and allergic health in schoolchildren. *Clin. Exp. Allergy* 35 (10), 1279-1287, doi:10.1111/j.1365-2222.2005.02336.

Pérez, C., Nickovic, S., Baldasano, J.M., Sicard, M., Rocadenbosch, F., Cachorro, V.E., 2006a. A long Saharan dust event over the western Mediterranean: Lidar, sun photometer observations, and regional dust modeling. *J. Geophys. Res.* 111 (D15214), 1-16, doi:10.1029/2005JD006579.

Pérez, C., Nickovic, S., Pejanovic, G., Baldasano, J.M., Ozsoy, E., 2006b. Interactive dust-radiation modeling: A step to improve weather forecasts. *J. Geophys. Res.* 111 (D16206), doi:10.1029/2005JD006717, 1-17.

Querol, X., Alastuey, A., Moreno, T., Viana, M.M., Castillo, S., Pey, J., Rodríguez, S., Artiñano, B.A., Salvador, P., Sánchez, M., Santos, S.G.D., Garraleta, M.D.H., Fernandez-Patier, R., Moreno-Grau, S., Negral, L., Minguillón, M.C., Monfort, E., Sanz, M.J., Palomo-Marín, R., Pinilla-Gil, E., Cuevas, E., de la Rosa, J., de la Campa, A.S., 2008. Spatial and temporal variations in airborne particulate matter (PM₁₀ and PM_{2.5}) across Spain 1999-2005. *Atmos. Environ.* 42 (17), 396-3979, doi:10.1016/j.atmosenv.2006.10.071.

Querol, X., Alastuey, A., Rodríguez, S., Plana, F., Ruiz, C.R., Cots, N., Massagué, G., Puig, O., 2001. PM₁₀ and PM_{2.5} source apportionment in the Barcelona metropolitan area, Catalonia, Spain. *Atmos. Environ.* 35 (36), 6407-6419.

Querol, X., Alastuey, A., Rodríguez, S., Viana, M.M., Artiñano, B.A., Salvador, P., Mantilla, E., Santos, S.G.D., Patier, R.F., Rosa, J.D.L., Campa, A.S.D.L., Menedez, M., 2003. Estudio y evaluación de la contaminación atmosférica por material particulado en España: Informes finales. Technical Report. IJA CSIC, ISCIII, CIEMAT, Universidad de Huelva, Universidad del País Vasco.

Querol, X., Alastuey, A., Rodríguez, S., Viana, M.M., Artiñano, B.A., Salvador, P., Mantilla, E., do Santos, S.G., Patier, R.F., de La Rosa, J., de la Campa, A.S., Menéndez, M., Gil, J.J., 2004a. Levels of particulate matter in rural, urban and industrial sites in Spain. *Sci. Tot. Env.* 334-335, 359-376, doi:10.1016/j.scitotenv.2004.04.036.

Querol, X., Alastuey, A., Ruiz, C.R., Artiñano, B., Hansson, H.C., Harrison, R.M., Buringh, E., ten Brink, H.M., Lutz, M., Bruckmann, P., Straehl, P., Schneider, J., 2004b. Speciation and origin of PM₁₀ and PM_{2.5} in selected European cities. *Atmos. Environ.* 38, 6547-6555.

Rauterberg-Wulff, 2000. Untersuchung über die Bedeutung der Staubaufwirbelung für die PM₁₀-Immission an einer Hauptverkehrsstraße. Technical Report. Techn. Univ. Berlin, Fachgebiet Luftreinhaltung.

Rodríguez, S., Querol, X., Alastuey, A., Plana, F., 2002. Sources and processes affecting levels and composition of atmospheric aerosol in the western Mediterranean. *J. Geophys. Res.* 107 (D24), 4777.

Russell, A., Dennis, R., 2000. NARSTO critical review of photochemical models and modeling. *Atmos. Environ.* 34 (12-14), 2283-2324, doi:10.1016/S1352-2310(99)00468-9.

San José, R., Rodriguez, M.A., Cortés, E., González, R.M., 1999. Emma model: an advanced operational mesoscale air quality model for urban and regional environments. *Environ. Manag. Health* 10 (4), 258-266.

Schell, B., Ackermann, I.J., Hass, H., Binkowski, F.S., Ebel, A., 2001. Modeling the formation of secondary organic aerosol within a comprehensive air quality model system. *J. Geophys. Res.* 106 (D22), 28275-28293, doi:2001JD000384.

Seinfeld, J.H., Pandis, S.N., 1998. *Atmospheric Chemistry and Physics*. John Wiley & Sons, New York, Chichester, Weinheim.

Skamarock, W.C., Klemp, J.B., 2008. A time-split nonhydrostatic atmospheric model for weather research and forecasting applications. *J. Comput. Phys.* 227

(7), 3465-3485, doi:10.1016/j.jcp.2007.01.037.

Slemr, F., Seiler, W., 1984. Field measurement of NO and NO₂ emissions from fertilized and unfertilized soils. *J. Atmos. Chem.* 2, 1-24.

Smith, S.N., Mueller, S.F., 2010. Modeling natural emissions in the community multiscale air quality (CMAQ) model - part 1: Building an emissions data base. *Atmos. Chem. Phys. Discuss.* 10, 1755-1821.

Stein, A., Mantilla, E., Millán, M., 2005. Using measured and modeled indicators to assess ozone-NO_x-VOC sensitivity in a western Mediterranean coastal environment. *Atmos. Environ.* 39, 7167-7180.

Talbot, R.W., Harriss, R.C., Browell, E.V., Gregory, G.L., Sebacher, D.I., Beck, S.M., 1986. Distribution and geochemistry of aerosols in the tropical north atlantic troposphere: Relationship to Saharan dust. *J. Geophys. Res.* 91 (D4), 51735182.

US-EPA, 1984. Interim procedures for evaluating air quality models (revised). Technical Report. EPA-450/4-91-013. U.S. Environmental Protection Agency, Office of Air Quality Planning and Standards: Research Triangle Park, NC.

US-EPA, 1991. Guideline for regulatory application of the urban airshed model. Technical Report. EPA-450/4-91-013. U.S. Environmental Protection Agency, Office of Air Quality Planning and Standards: Research Triangle Park, NC.

US-EPA, 1997. AP-42, 5. Edition, Volume 1, Chapter 13, Section 13.2.1. Miscellaneous sources. Technical Report. U.S. Environmental Protection Agency.

US-EPA, 2007. AP-42. 5th Edition, Volume VI, Chapter 13, Section 13.2.1. Paved Roads. Technical Report. U.S.-Environmental Protection Agency. US-EPA, 2007. Guidance on the Use of Models and Other Analyses for Demonstrating Attainment of Air Quality Goals for Ozone, PM_{2.5}, and Regional Haze. Technical Report. EPA-454/B-07-002. U.S. Environmental Protection Agency, Office of Air Quality Planning and Standards: Research Triangle Park, NC.

Vautard, R., Bessagnet, B., Chin, M., Menut, L., 2005a. On the contribution of natural aeolian sources to particulate matter concentrations in Europe: Testing hypotheses with a modelling approach. *Atmos. Environ.* 39 (18), 3291-3303, doi:10.1016/j.atmosenv.2005.01.051.

Vautard, R., Honoré, C., Beekmann, M., Rouïl, L., 2005b. Simulation of ozone during the august 2003 heat wave and emission control scenarios. *Atmos. Environ.* 39 (16), 2957-2967, doi:10.1016/j.atmosenv.2005.01.039.

Venkatram, A., 2000. A critique of empirical emission factor models: a case study of the AP-42 model for estimating pm₁₀ emissions from paved roads.

Atmos. Environ. 34, 1-11.

Venkatram, A., Pleim, J., 1999. The electrical analogy does not apply to modeling dry deposition of particles. *Atmos. Environ.* 33 (18), 3075-3076, doi:10.1016/S1352-2310(99)00094-1.

Viana, M., Pérez, C., Querol, X., Alastuey, A., Nickovic, S., Baldasano, J.M., 2005. Spatial and temporal variability of PM levels and composition in a complex summer atmospheric scenario in Barcelona (NE Spain). *Atmos. Environ.* 39, 5343-5361.

Vivanco, M.G., Correa, M., Azula, O., Palomino, I., Martín, F., 2008. Influence of model resolution on ozone predictions over Madrid area (Spain), in: *Computer Science, L.N. (Ed.), Computational Science and Its Applications ICCSA 2008*, Springer Berlin/Heidelberg. pp. 165-178.

Vivanco, M.G., Palomino, I., Vautard, R., Bessagnet, B., Martín, F., Menut, L., Jiménez, S., 2009. Multi-year assessment of photochemical air quality simulation over Spain. *Environ. Modell. Softw.* 24, 63-73.

Weil, J.C., Sykes, R.I., Venkatram, A., 1992. Evaluating air-quality models: review and outlook. *J. Appl. Met.* 31, 1121-1145.

Zhang, K., Knipping, E., Wexler, A., Bhave, P., Tonnesen, G., 2005. Size distribution of sea-salt emissions as a function of relative humidity. *Atmos. Environ.* 39, 3373-3379.

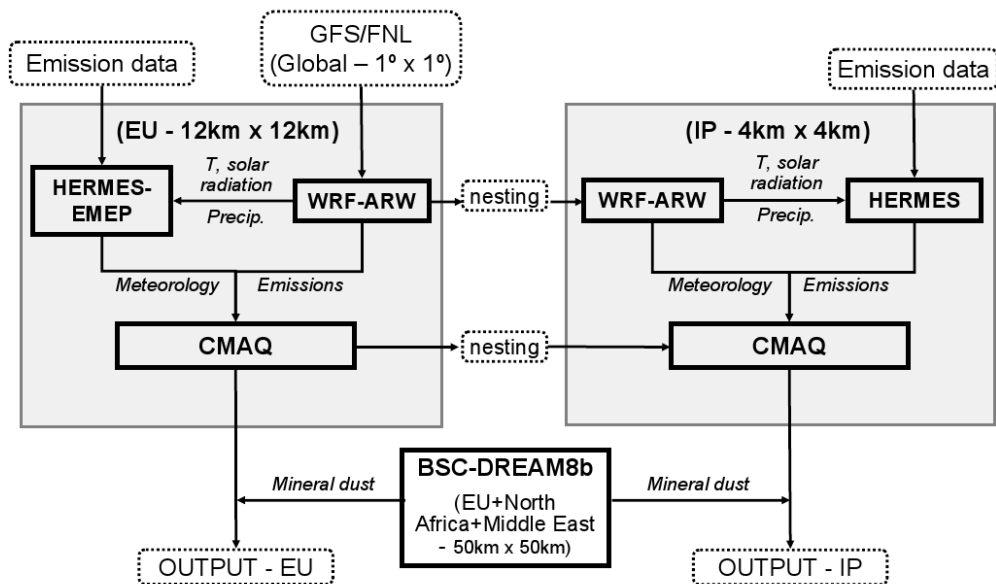


Figure 1: Modular structure of the CALIOPE modeling system used to simulate air quality dynamics in Spain. Squared boxes with solid lines represent the main models of the framework. Boxes with dashed lines represent input/output dataset. Lines connecting boxes represent the information flow.

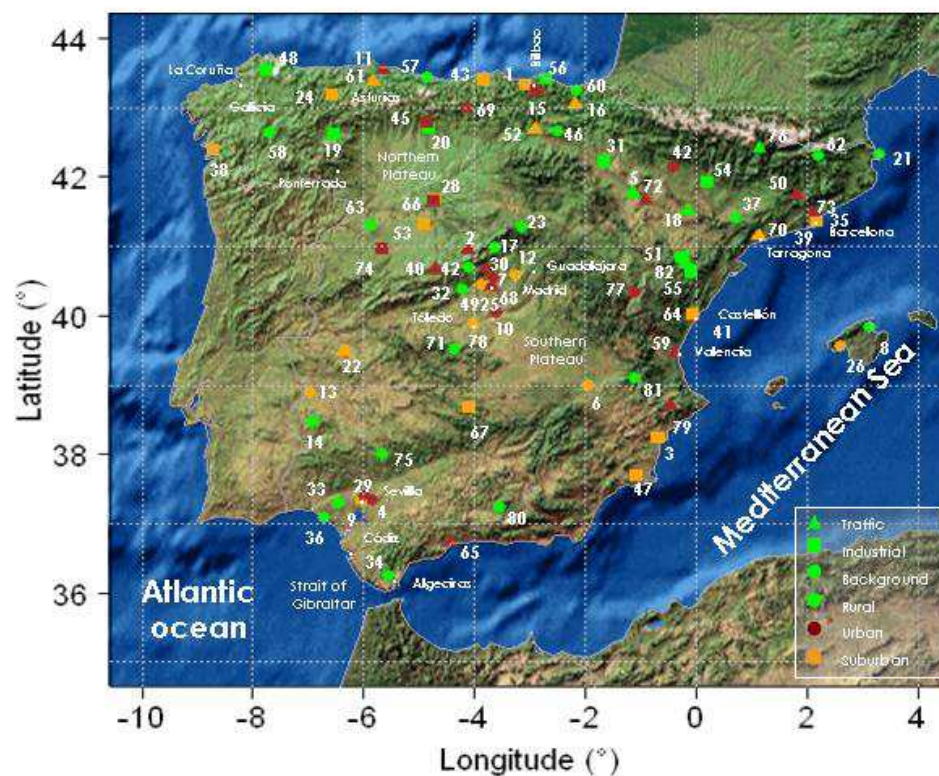


Figure 2: RedESP stations measuring air pollutants in Spain on an hourly basis in 2004. Different types of stations (U: Urban; S: Suburban; R: Rural; B: Background; I: Industrial; and T: Traffic) according to Garber et al. (2002) are represented by symbols and color codes. The various symbols represent the major emission types affecting each station (Traffic: triangle; Industrial: square; and Background: circle) while the colors reflect the environment of each station (Urban: red; Suburban: green; and Rural: orange). Characteristics and number of each station are listed in Tab. 1.

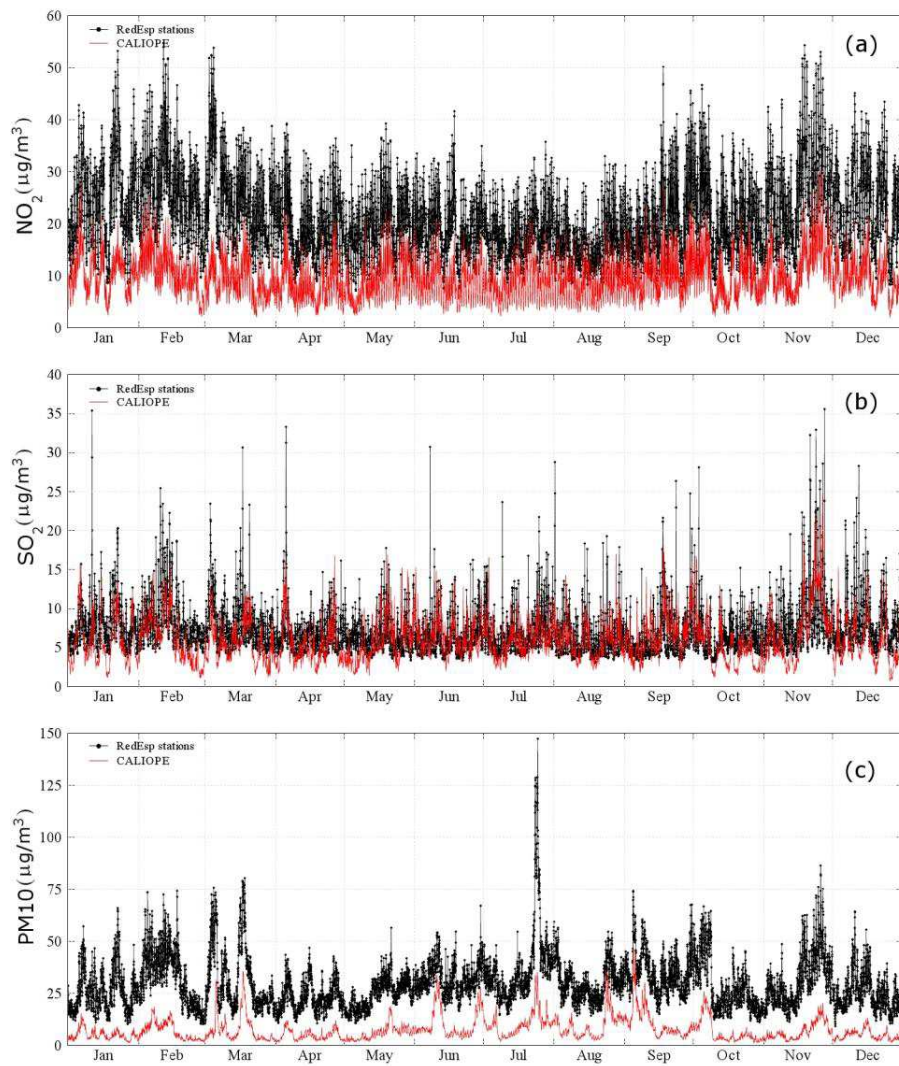


Figure 3: Modeled (red lines) and measured (marked black lines) time series of hourly mean concentrations (in $\mu\text{g m}^{-3}$) for NO_2 (a), SO_2 (b) and PM_{10} (c), respectively, at the RedESP stations.

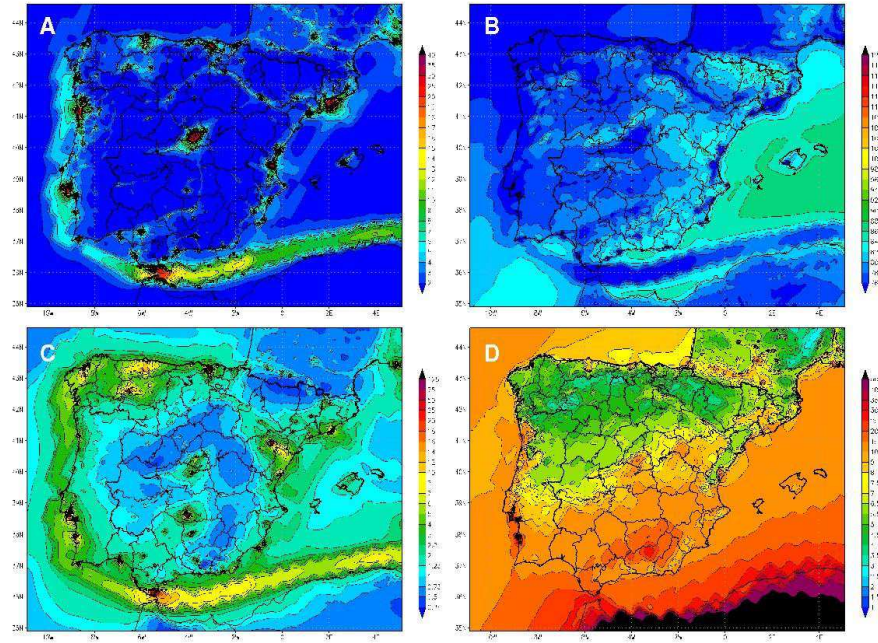


Figure 4: 2004 annual average concentrations ($\mu\text{g m}^{-3}$) of (a) NO₂, (b) O₃, (c) SO₂, (d) PM₁₀ at ground level simulated by CALIOPE over Spain at a 4 km x 4 km spatial resolution.

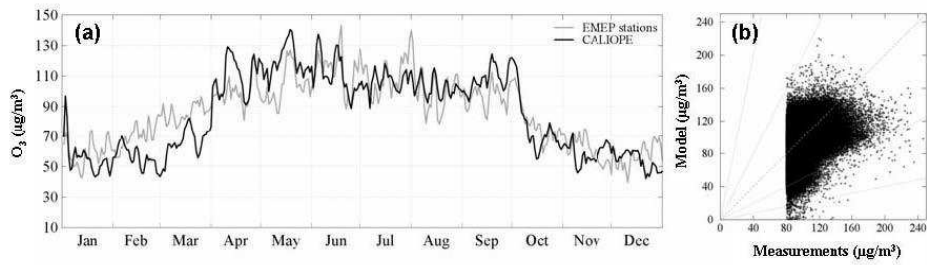


Figure 5: Modeled (black lines) and measured (grey lines) time series of daily peak concentrations (a) and scatter plots in hourly basis (b) for O₃ at the RedESP stations. The scatter plot includes the 1:1, 1:2, 1:5, and 5:1 reference lines. A cut-off value of 80 µg m⁻³ is applied to the observation in the scatter plot.

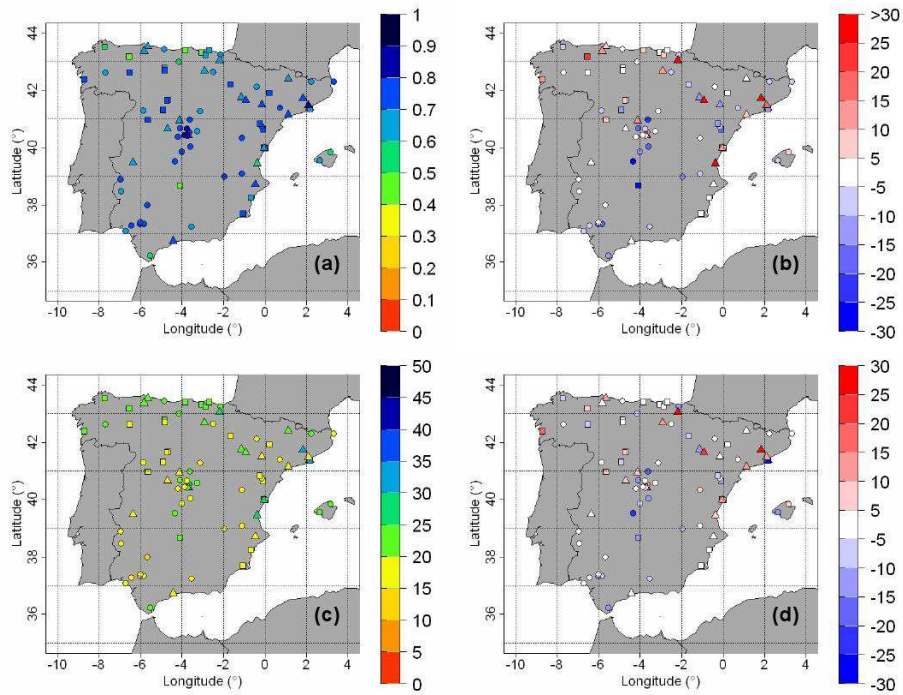


Figure 6: Spatial distribution of the statistics for O₃ over 2004 at the RedESP stations: daily peak correlation coefficient (r) (a), annual Mean Bias (MB, in $\mu\text{g m}^{-3}$) for daily peak (b), Mean Normalized Gross Error (MNGE, in %) in hourly basis (c), and Mean Normalized Bias Error (MNBE, in %) in hourly basis (d). Note that MB, MNGE and MNBE are calculated with a $80 \mu\text{g m}^{-3}$ cut-off according to US-EPA (1991) and Russell and Dennis (2000).

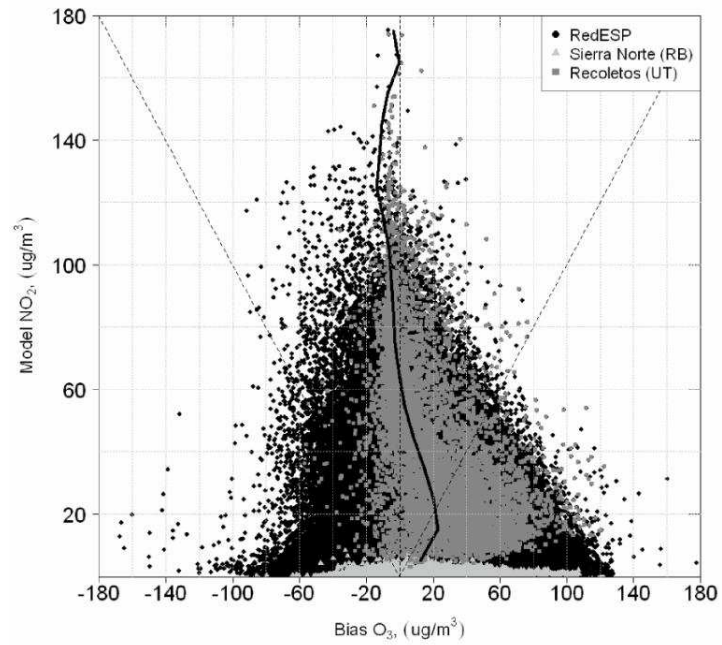


Figure 7: Modeled NO₂ levels versus model-observation O₃ bias. The 68 stations measuring both NO₂ and O₃ are represented on an hourly basis (black dots). Data from Sierra Norte, a rural background station (light grey triangles) and Recoletos, urban traffic (dark grey squares) are also displayed. The vertical black curve represents the average concentration on the X-axis every 10 $\mu\text{g m}^{-3}$ from the vertical axis.

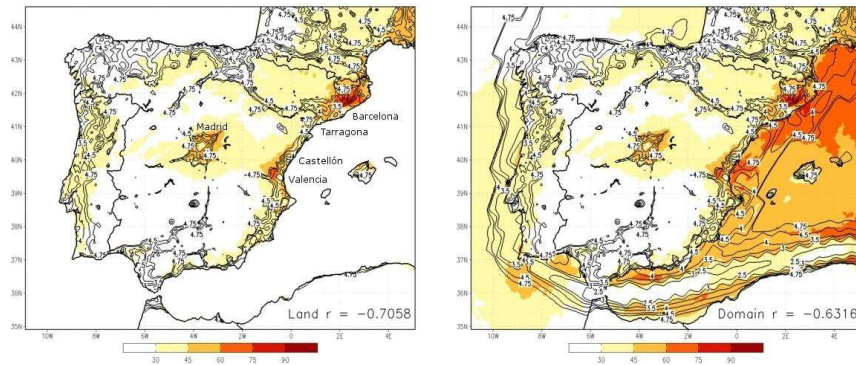


Figure 8: Days exceeding the concentration value of $120 \mu\text{g m}^{-3}$ for the 8-hr maximum O_3 concentration (color scale) and the logarithm of the VOCs/ NO_x concentration ratio (contour lines) during the high O_3 season (from April to September) in 2004 simulated by CALIOPE at a $4 \text{ km} \times 4 \text{ km}$ over the land domain (a) and the entire domain (b). In both cases, correlation between days exceeding the concentration value of $120 \mu\text{g m}^{-3}$ and the logarithm of the VOCs/ NO_x concentration ratio is showed at the bottom-right.

Table 1: Location and characteristics of selected RedESP stations (source: CEAM) for 2004 on an hourly basis. 68 stations were used to monitor NO₂, 45 for SO₂, 82 for O₃, and 44 for PM₁₀, respectively.

	Station name	Latitude ^a	Longitude ^a	Altitude (m)	Type ^b	Hourly concentration			
						NO ₂	SO ₂	O ₃	PM ₁₀
1	Abanto	+43.322	-3.073	75	SI	x	x	x	x
2	Acueducto	+40.950	-4.116	1002	UT	x		x	x
3	Agro	+38.242	-0.683	44	SI	x	x		
4	Al.Guadaira	+37.342	-5.833	68	UB	x		x	x
5	Alagón	+41.763	-1.143	235	RT	x	x	x	
6	Albacete	+38.981	-1.957	686	SB	x	x	x	x
7	Alcobendas(R.)	+40.541	-3.646	688	UB	x	x	x	x
8	Alcudial–Alc	+39.838	+3.147	15	RB	x		x	
9	Aljarafe	+37.340	-6.043	68	SB	x	x	x	x
10	Aranjuez	+40.034	-3.592	501	UB	x		x	x
11	Av.Castilla	+43.538	-5.646	7	UT	x	x	x	x
12	Azuqueca	+40.574	-3.263	662	SB	x	x	x	x
13	Badajoz	+38.892	-6.970	390	SB	x		x	x
14	Barcarrota	+38.476	-6.923	393	RB	x	x	x	
15	Basauri	+43.240	-2.881	125	UI	x	x	x	x
16	Beasain	+43.048	-2.191	153	ST	x		x	x
17	Buitrago	+40.979	-3.622	1024	RB			x	
18	Bujaralo	+41.505	-0.152	327	RT	x		x	
19	C.T. Compos1	+42.626	-6.521	720	RI	x		x	x
20	C.T. Guardo2	+42.704	-4.827	1065	RI			x	
21	Cabo de Creus	+42.319	+3.316	23	RB	x	x	x	
22	Cáceres	+39.482	-6.357	389	ST	x		x	x
23	Campisábalos	+41.281	-3.143	1360	RB	x	x	x	
24	Cangas	+43.181	-6.550	330	SI	x	x	x	x
25	Casa Campo	+40.420	-3.750	645	SB	x		x	x
26	Cast. Bellver	+39.564	+2.623	117	SB	x	x	x	x
27	Castellón	+39.983	-0.045	28	UT	x	x	x	x
28	Cementerio	+41.674	-4.697	695	SI	x		x	
29	Centro	+37.389	-5.992	19	UB			x	
30	Colmenar	+40.665	-3.774	905	UB	x		x	x
31	CTCC-Arguedas	+42.225	-1.667	490	RI	x	x	x	x
32	Chapinería	+40.378	-4.205	675	RB	x		x	x
33	Doñana	+37.285	-6.440	20	RB	x		x	x
34	E2 Alcornocales	+36.234	-5.540	189	RB			x	
35	Eixample	+41.386	+2.154	12	UT	x	x	x	
36	El Arenosillo	+37.088	-6.705	37	RB			x	
37	Els Torm	+41.395	+0.721	470	RB	x	x	x	
38	Esc.Naval	+42.395	-8.708	20	SI		x	x	
39	Escullera	+41.353	+2.177	16	SI			x	
40	Estacion	+40.657	-4.690	1150	UT	x		x	x
41	Grao	+39.984	+0.009	10	SI	x	x	x	
42	Guadarrá	+40.679	-4.105	1025	RB			x	
43	Guarnizo	+43.404	-3.842	16	SI	x	x	x	x
44	Huesca	+42.136	-0.404	488	UB			x	
45	Instituto	+42.792	-4.847	1120	UI	x	x	x	x
46	Izkiz	+42.653	-2.501	810	RB	x	x	x	x
47	La Aljorra	+37.694	-1.068	80	SI	x		x	x
48	Louseiras	+43.536	-7.740	540	RI	x	x	x	x
49	Majadahonda	+40.446	-3.868	730	SB	x		x	x
50	Manresa	+41.731	1.826	238	UT	x		x	
51	Mas Matas	+40.841	-0.249	510	RI	x	x	x	x

Table 1: Continue

	Station name	Latitude ^a	Longitude ^a	Altitude (m)	Type ^b	Hourly concentration			
						NO ₂	SO ₂	O ₃	PM ₁₀
52	Mda. de Ebro1	+42.682	-2.918	471	ST			x	
53	Medina	+41.316	-4.909	721	SI	x		x	x
54	Monzón	+41.918	+0.197	279	RI			x	
55	Morella	+40.636	-0.093	1150	RI	x	x	x	x
56	Mundaka	+43.406	-2.704	116	RI	x	x	x	x
57	Niembro	+43.439	-4.850	134	RB	x	x	x	
58	O Saviñao	+42.635	-7.705	506	RB	x	x	x	
59	P. Silla	+39.458	-0.377	11	UT	x	x	x	
60	Pagoeta	+43.251	-2.155	215	RB	x		x	x
61	Pal. Deportes	+43.367	-5.831	206	ST	x	x	x	x
62	Pardines	+42.312	+2.214	1224	RB		x	x	
63	Penausende	+41.289	-5.867	985	RB	x	x	x	
64	Peneta	+40.013	-0.058	106	SI	x	x	x	
65	Ps. Martiricos	+36.729	-4.427	4	UT	x		x	x
66	Pte. Regeral	+41.654	-4.735	691	UI	x	x	x	x
67	Puertollano	+38.683	-4.089	670	SI	x	x	x	x
68	Recoletos	+40.423	-3.692	648	UT	x	x	x	x
69	Reinosa	+43.001	-4.136	851	UB	x	x	x	x
70	Reus	+41.151	+1.120	103	ST	x	x	x	
71	Risco Llano	+39.523	-4.353	1241	RB	x	x	x	
72	Roger Flor	+41.651	-0.917	212	UT	x		x	x
73	S. Cugat	+41.481	+2.090	113	UT	x	x	x	
74	Salamanca2	+40.965	-5.656	797	UI	x	x	x	
75	Sierra Norte	+37.996	-5.666	569	RB	x		x	x
76	Sort	+42.407	+1.130	692	RT		x	x	
77	Teruel	+40.336	-1.107	915	UB			x	
78	Toledo	+39.867	-4.021	500	SB	x		x	x
79	Verge	+38.707	-0.467	534	UT	x	x	x	
80	Víznar	+37.237	-3.534	1230	RB	x	x	x	
81	Zarra	+39.086	-1.102	885	RB	x	x	x	
82	Zorita	+40.734	-0.169	619	RB	x	x	x	x

^a A positive value indicates northern latitudes or eastern longitudes. A negative value indicates southern latitudes or western longitudes.

^b U: Urban; S: Suburban; R: Rural; B: Background; I: Industrial; T: Traffic. See Garber et al. (2002).

Table 2: Annual statistics obtained with CALIOPE over Spain for 2004 at the RedESP stations. The calculated statistics are: measured mean ($\mu\text{g m}^{-3}$), modeled mean ($\mu\text{g m}^{-3}$), correlation coefficient (r), Root Mean Square Error (RMSE, $\mu\text{g m}^{-3}$), Mean Fractional Bias (MFB, %) and Error (MFE, %). All metrics are calculated without cut-off value.

Pollutant	Category	Number of stations	Measured mean	Modeled mean	r	RMSE	MFB	MFE
NO ₂ hourly	All	68	21.6	9.6	0.53	23.3	-81.1	98.8
	Rural	25	7.6	3.3	0.51	7.6	-79.7	95.6
	Suburban	22	23.2	11.7	0.39	23.1	-66.7	93.6
	Urban	21	36.5	14.8	0.47	33.6	-97.7	107.9
SO ₂ hourly	All	45	7.2	6.1	0.19	18.7	-33.1	97.8
	Rural	18	4.4	3.3	0.28	14.0	-29.9	94.1
	Suburban	14	9.1	9.9	0.14	26.0	-23.8	95.5
	Urban	13	9.3	6.0	0.14	15.1	-47.1	105.4
PM10 hourly	All	44	29.6	7.5	0.38	33.4	-111.8	119.8
	Rural	12	19.6	5.9	0.43	20.4	-96.0	110.4
	Suburban	17	35.0	8.0	0.36	39.7	-118.6	123.6
	Urban	15	31.8	8.1	0.36	33.8	-116.3	122.9

Table 3: Annual statistics for O₃ (hourly and daily peaks) obtained with CALIOPE over Spain for 2004 at the RedESP stations. The calculated statistics are: measured mean ($\mu\text{g m}^{-3}$), modeled mean ($\mu\text{g m}^{-3}$), correlation coefficient (r), Root Mean Square Error (RMSE, $\mu\text{g m}^{-3}$), Mean Fractional Bias (MFB, %) and Error (MFE; %), Mean Normalized Bias Error (MNBE, %) and Gross Error (MNGE; %). All metrics, except for r , are calculated with a $80 \mu\text{g m}^{-3}$ cut-off value (see US-EPA, 1991; Russell and Dennis, 2000).

Pollutant	Category	Number of stations	Measured mean	Modeled mean	r	RMSE	MFB	MFE	MNBE	MNGE
O ₃ hourly	All	82	57.4	71.0	0.57	24.1	-9.3	21.2	-6.0	19.2
	Rural	33	70.1	76.2	0.51	24.1	-11.2	21.8	-7.7	19.5
	Suburban	25	51.7	67.5	0.56	24.7	-8.7	20.7	-5.4	18.9
	Urban	24	45.4	67.4	0.60	23.4	-4.2	19.8	-1.2	18.9
O ₃ peaks	All	82	86.1	85.5	0.64	25.9	-9.8	21.2	-6.6	19.5
	Rural	33	93.8	86.9	0.67	24.8	-12.9	21.3	-9.7	19.0
	Suburban	25	84.7	84.1	0.65	27.9	-9.0	21.5	-5.7	19.9
	Urban	24	76.6	85.0	0.63	25.8	-4.2	20.7	-1.0	20.0

Table 1

[Click here to download Table: Table1.doc](#)Table 1: Location and characteristics of selected RedESP stations (source: CEAM) for 2004 on an hourly basis. 68 stations were used to monitor NO₂, 45 for SO₂, 82 for O₃, and 44 for PM₁₀, respectively.

	Station name	Latitude ^a	Longitude ^a	Altitude (m)	Type ^b	Hourly concentration			
						NO ₂	SO ₂	O ₃	PM ₁₀
1	Abanto	+43.322	-3.073	75	SI	x		x	x
2	Acueducto	+40.950	-4.116	1002	UT	x		x	x
3	Agro	+38.242	-0.683	44	SI	x	x	x	
4	Al.Guadaira	+37.342	-5.833	68	UB	x		x	x
5	Alagón	+41.763	-1.143	235	RT	x	x	x	
6	Albacete	+38.981	-1.957	686	SB	x	x	x	x
7	Alcobendas(R.)	+40.541	-3.646	688	UB	x	x	x	x
8	Alcudial...Alc	+39.838	+3.147	15	RB	x		x	
9	Aljarafe	+37.340	-6.043	68	SB	x	x	x	x
10	Aranjuez	+40.034	-3.592	501	UB	x		x	x
11	Av.Castilla	+43.538	-5.646	7	UT	x	x	x	x
12	Azuqueca	+40.574	-3.263	662	SB	x	x	x	x
13	Badajoz	+38.892	-6.970	390	SB	x		x	x
14	Barcarrota	+38.476	-6.923	393	RB	x	x	x	
15	Basauri	+43.240	-2.881	125	UI	x	x	x	x
16	Beasain	+43.048	-2.191	153	ST	x		x	x
17	Buitrago	+40.979	-3.622	1024	RB			x	
18	Bujaralo	+41.505	-0.152	327	RT	x		x	
19	C.T. Compos1	+42.626	-6.521	720	RI	x			x
20	C.T. Guardo2	+42.704	-4.827	1065	RI			x	
21	Cabo de Creus	+42.319	+3.316	23	RB	x	x	x	
22	Cáceres	+39.482	-6.357	389	ST	x		x	x
23	Campisábalos	+41.281	-3.143	1360	RB	x	x	x	
24	Cangas	+43.181	-6.550	330	SI	x	x	x	x
25	Casa Campo	+40.420	-3.750	645	SB	x		x	x
26	Cast. Bellver	+39.564	+2.623	117	SB	x	x	x	x
27	Castellón	+39.983	-0.045	28	UT	x	x	x	x
28	Cementerio	+41.674	-4.697	695	SI	x		x	
29	Centro	+37.389	-5.992	19	UB			x	
30	Colmenar	+40.665	-3.774	905	UB	x		x	x
31	CTCC-Arguedas	+42.225	-1.667	490	RI	x	x	x	x
32	Chapinerfa	+40.378	-4.205	675	RB	x		x	x
33	Doñana	+37.285	-6.440	20	RB	x		x	x
34	E2 Alcornocales	+36.234	-5.540	189	RB			x	
35	Eixample	+41.386	+2.154	12	UT	x	x	x	
36	El Arenosillo	+37.088	-6.705	37	RB			x	
37	Els Torm	+41.395	+0.721	470	RB	x	x	x	
38	Esc.Naval	+42.395	-8.708	20	SI		x	x	
39	Escullera	+41.353	+2.177	16	SI			x	
40	Estacion	+40.657	-4.690	1150	UT	x		x	x
41	Grao	+39.984	+0.009	10	SI	x	x	x	
42	Guadarra	+40.679	-4.105	1025	RB			x	
43	Guarnizo	+43.404	-3.842	16	SI	x	x	x	x
44	Huesca	+42.136	-0.404	488	UB			x	
45	Instituto	+42.792	-4.847	1120	UI	x	x	x	x
46	Izkiz	+42.653	-2.501	810	RB	x	x	x	x
47	La Aljorra	+37.694	-1.068	80	SI	x		x	x
48	Louseiras	+43.536	-7.740	540	RI	x	x	x	x
49	Majadahonda	+40.446	-3.868	730	SB	x		x	x
50	Manresa	+41.731	1.826	238	UT	x		x	
51	Mas Matas	+40.841	-0.249	510	RI	x	x	x	x

Table 1: Continue

	Station name	Latitude ^a	Longitude ^a	Altitude (m)	Type ^b	Hourly concentration			
						NO ₂	SO ₂	O ₃	PM ₁₀
52	Mda. de Ebro1	+42.682	-2.918	471	ST			x	
53	Medina	+41.316	-4.909	721	SI	x		x	x
54	Monzón	+41.918	+0.197	279	RI			x	
55	Morella	+40.636	-0.093	1150	RI	x	x	x	x
56	Mundaka	+43.406	-2.704	116	RI	x	x	x	x
57	Niembro	+43.439	-4.850	134	RB	x	x	x	
58	O Saviñao	+42.635	-7.705	506	RB	x	x	x	
59	P. Silla	+39.458	-0.377	11	UT	x	x	x	
60	Pagoeta	+43.251	-2.155	215	RB	x		x	x
61	Pal. Deportes	+43.367	-5.831	206	ST	x	x	x	x
62	Pardines	+42.312	+2.214	1224	RB		x	x	
63	Penausende	+41.289	-5.867	985	RB	x	x	x	
64	Peneta	+40.013	-0.058	106	SI	x	x	x	
65	Ps. Martiricos	+36.729	-4.427	4	UT	x		x	x
66	Pte. Regeral	+41.654	-4.735	691	UI	x	x	x	x
67	Puertollano	+38.683	-4.089	670	SI	x	x	x	x
68	Recoletos	+40.423	-3.692	648	UT	x	x	x	x
69	Reinosa	+43.001	-4.136	851	UB	x	x	x	x
70	Reus	+41.151	+1.120	103	ST	x	x	x	
71	Risco Llano	+39.523	-4.353	1241	RB	x	x	x	
72	Roger Flor	+41.651	-0.917	212	UT	x		x	x
73	S. Cugat	+41.481	+2.090	113	UT	x	x	x	
74	Salamanca2	+40.965	-5.656	797	UI	x	x	x	
75	Sierra Norte	+37.996	-5.666	569	RB	x		x	x
76	Sort	+42.407	+1.130	692	RT		x	x	
77	Teruel	+40.336	-1.107	915	UB			x	
78	Toledo	+39.867	-4.021	500	SB	x		x	x
79	Verge	+38.707	-0.467	534	UT	x	x	x	
80	Víznar	+37.237	-3.534	1230	RB	x	x	x	
81	Zarra	+39.086	-1.102	885	RB	x	x	x	
82	Zorita	+40.734	-0.169	619	RB	x	x	x	x

^a A positive value indicates northern latitudes or eastern longitudes. A negative value indicates southern latitudes or western longitudes.

^b U: Urban; S: Suburban; R: Rural; B: Background; I: Industrial; T: Traffic. See Garber et al. (2002).

Table 2[Click here to download Table: Table2.doc](#)

Table 2: Annual statistics obtained with CALIOPE over Spain for 2004 at the RedESP stations. The calculated statistics are: measured mean ($\mu\text{g m}^{-3}$), modeled mean ($\mu\text{g m}^{-3}$), correlation coefficient (r), Root Mean Square Error (RMSE, $\mu\text{g m}^{-3}$), Mean Fractional Bias (MFB, %) and Error (MFE, %). All metrics are calculated without cut-off value.

Pollutant	Category	Number of stations	Measured mean	Modeled mean	r	RMSE	MFB	MFE
NO ₂ hourly	All	68	21.6	9.6	0.53	23.3	-81.1	98.8
	Rural	25	7.6	3.3	0.51	7.6	-79.7	95.6
	Suburban	22	23.2	11.7	0.39	23.1	-66.7	93.6
	Urban	21	36.5	14.8	0.47	33.6	-97.7	107.9
SO ₂ hourly	All	45	7.2	6.1	0.19	18.7	-33.1	97.8
	Rural	18	4.4	3.3	0.28	14.0	-29.9	94.1
	Suburban	14	9.1	9.9	0.14	26.0	-23.8	95.5
	Urban	13	9.3	6.0	0.14	15.1	-47.1	105.4
PM10 hourly	All	44	29.6	7.5	0.38	33.4	-111.8	119.8
	Rural	12	19.6	5.9	0.43	20.4	-96.0	110.4
	Suburban	17	35.0	8.0	0.36	39.7	-118.6	123.6
	Urban	15	31.8	8.1	0.36	33.8	-116.3	122.9

Table 3
[Click here to download Table: Table3.doc](#)

Table 3: Annual statistics for O₃ (hourly and daily peaks) obtained with CALIOPE over Spain for 2004 at the RedESP stations. The calculated statistics are: measured mean ($\mu\text{g m}^{-3}$), modeled mean ($\mu\text{g m}^{-3}$), correlation coefficient (r), Root Mean Square Error (RMSE, $\mu\text{g m}^{-3}$), Mean Fractional Bias (MFB, %) and Error (MFE; %), Mean Normalized Bias Error (MNBE, %) and Gross Error (MNGE; %). All metrics, except for r , are calculated with a $80 \mu\text{g m}^{-3}$ cut-off value (see US-EPA, 1991; Russell and Dennis, 2000).

Pollutant	Category	Number of stations	Measured mean	Modeled mean	r	RMSE	MFB	MFE	MNBE	MNGE
O ₃ hourly	All	82	57.4	71.0	0.57	24.1	-9.3	21.2	-6.0	19.2
	Rural	33	70.1	76.2	0.51	24.1	-11.2	21.8	-7.7	19.5
	Suburban	25	51.7	67.5	0.56	24.7	-8.7	20.7	-5.4	18.9
	Urban	24	45.4	67.4	0.60	23.4	-4.2	19.8	-1.2	18.9
O ₃ peaks	All	82	86.1	85.5	0.64	25.9	-9.8	21.2	-6.6	19.5
	Rural	33	93.8	86.9	0.67	24.8	-12.9	21.3	-9.7	19.0
	Suburban	25	84.7	84.1	0.65	27.9	-9.0	21.5	-5.7	19.9
	Urban	24	76.6	85.0	0.63	25.8	-4.2	20.7	-1.0	20.0

Figure 1

[Click here to download high resolution image](#)

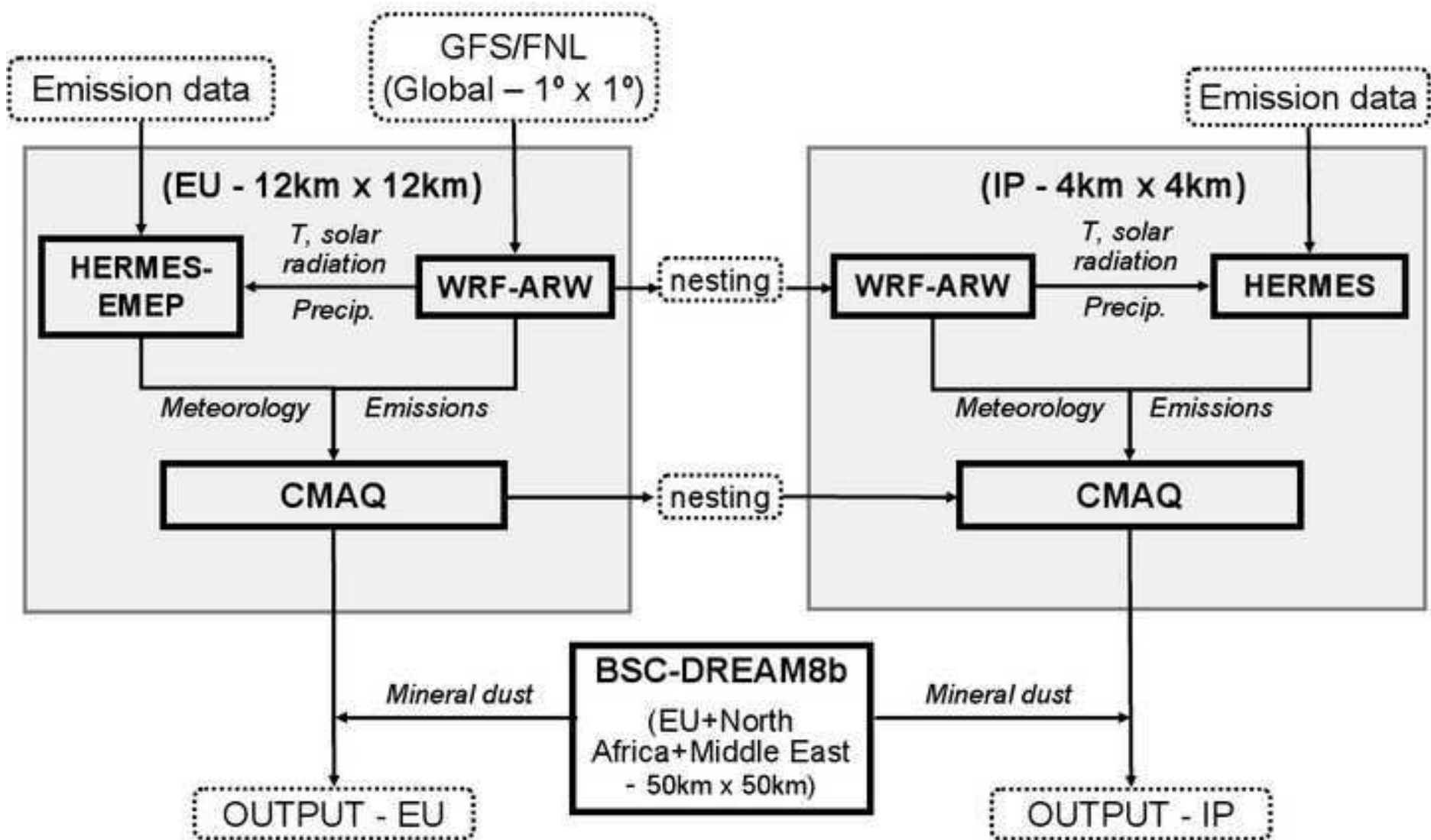


Figure 2

[Click here to download high resolution image](#)

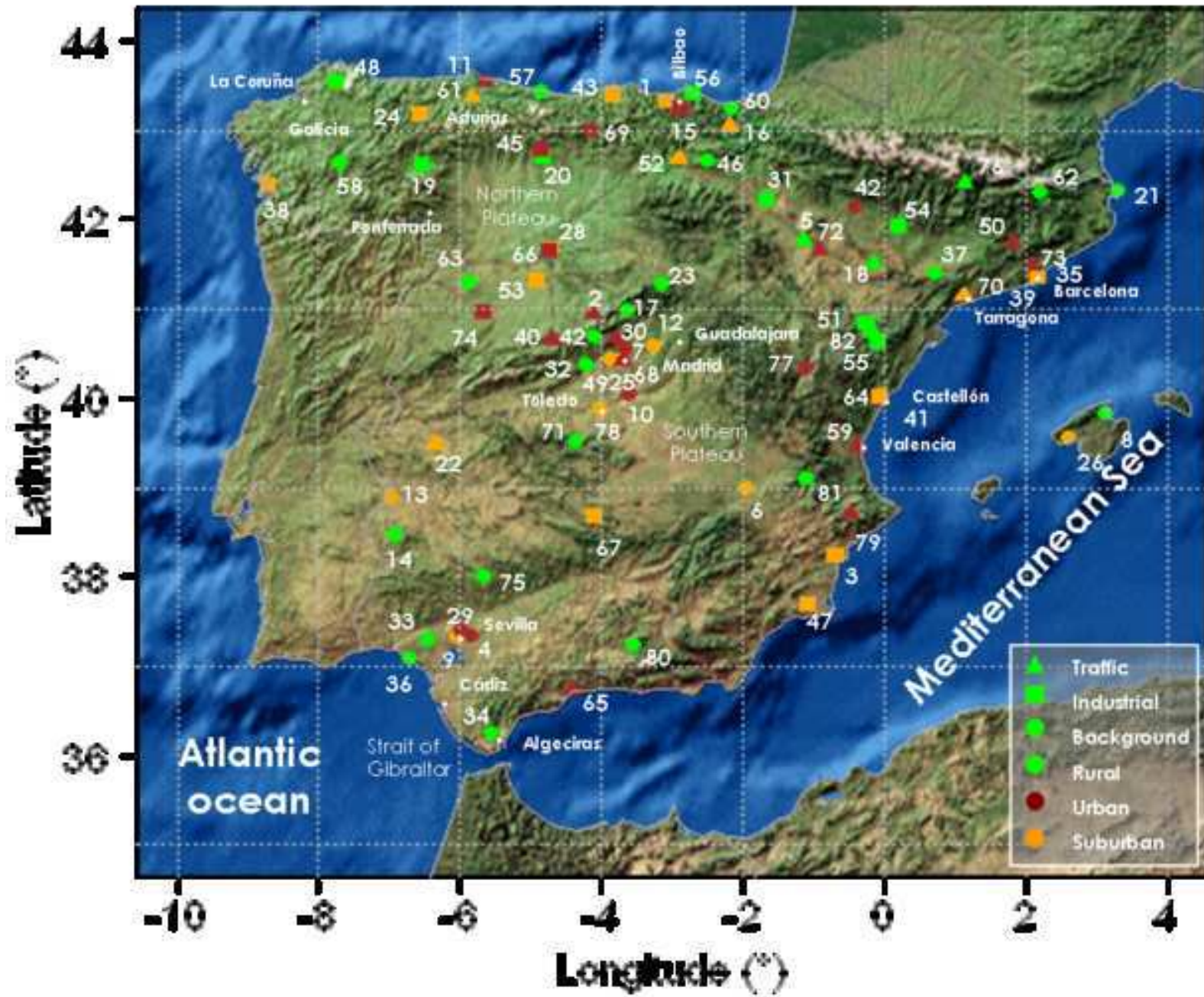


Figure 3
[Click here to download high resolution image](#)

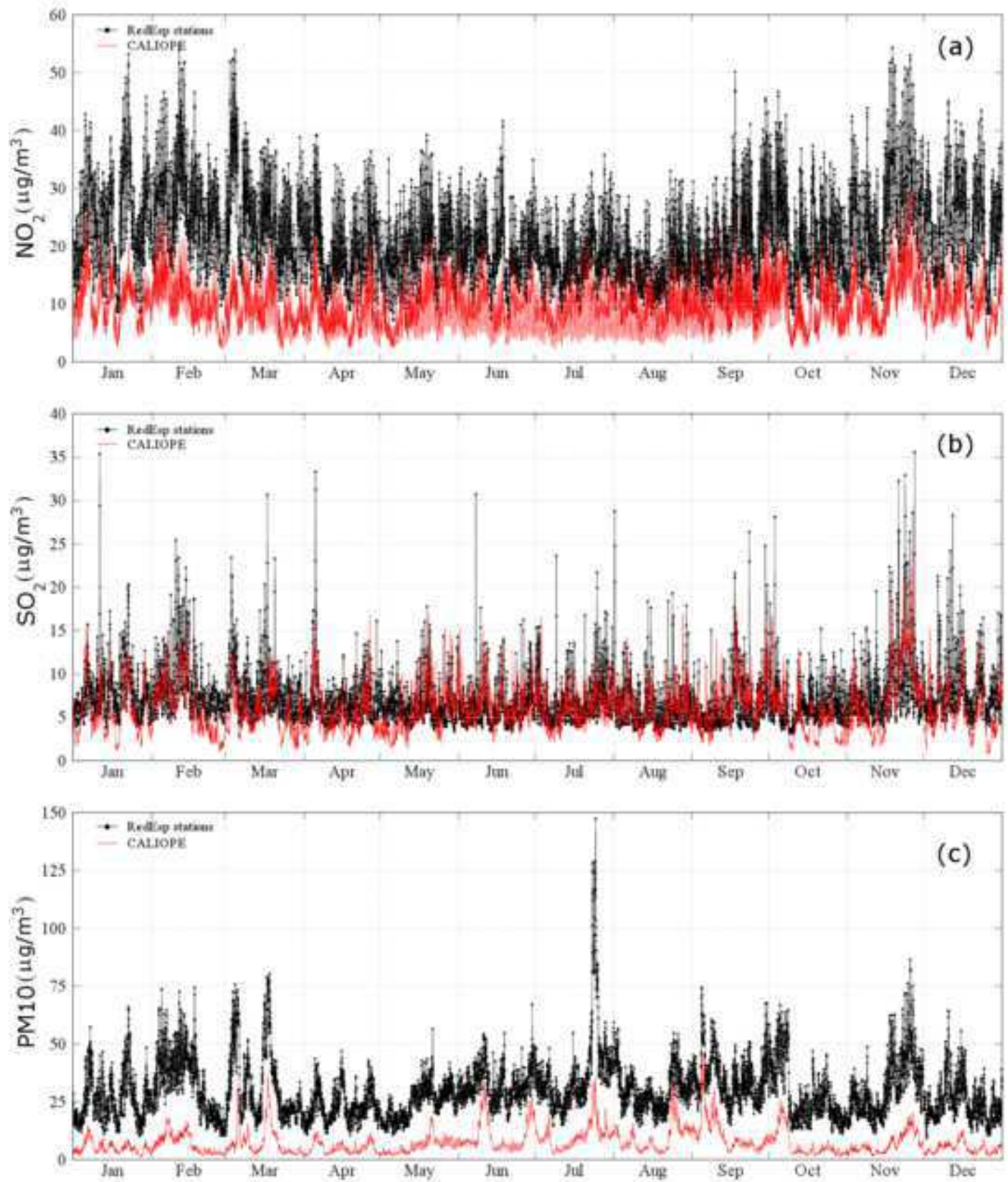


Figure 4

[Click here to download high resolution image](#)

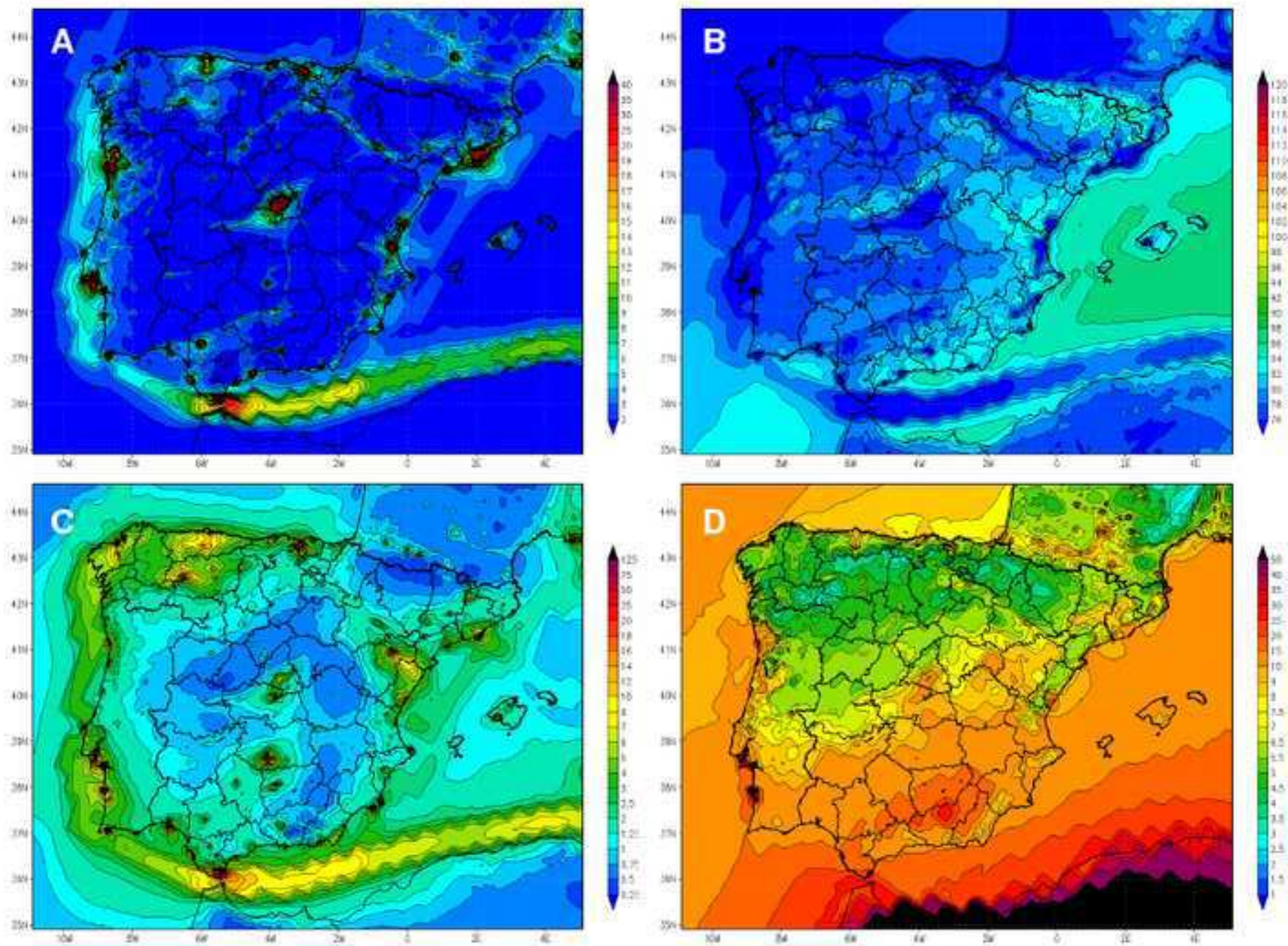


Figure 5

[Click here to download high resolution image](#)

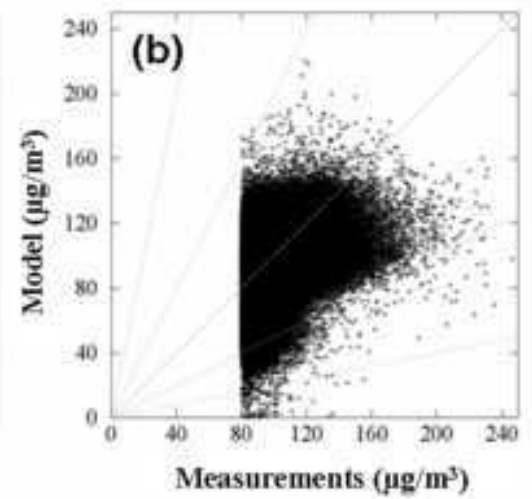
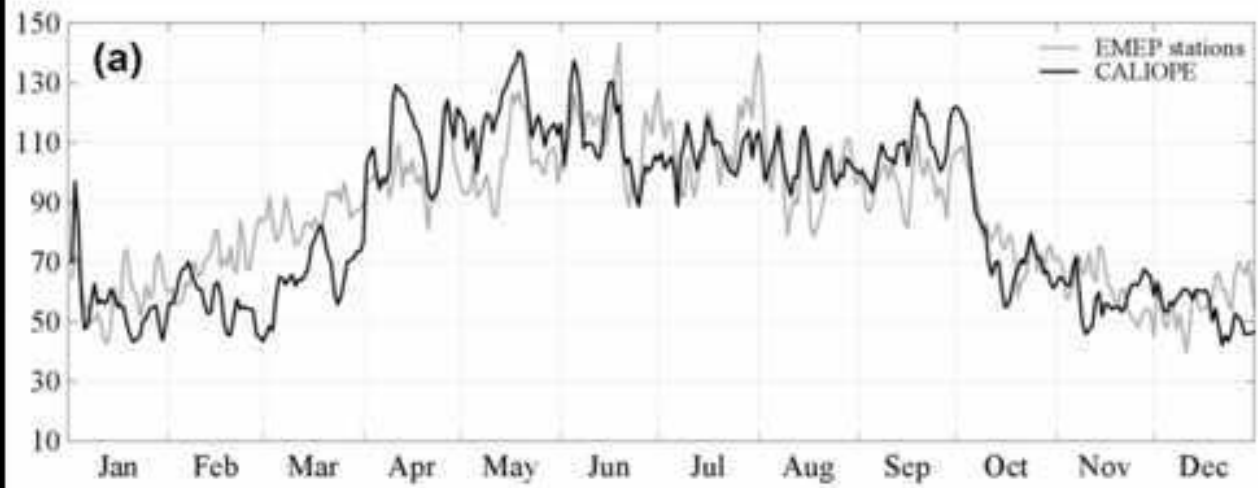


Figure 6

[Click here to download high resolution image](#)

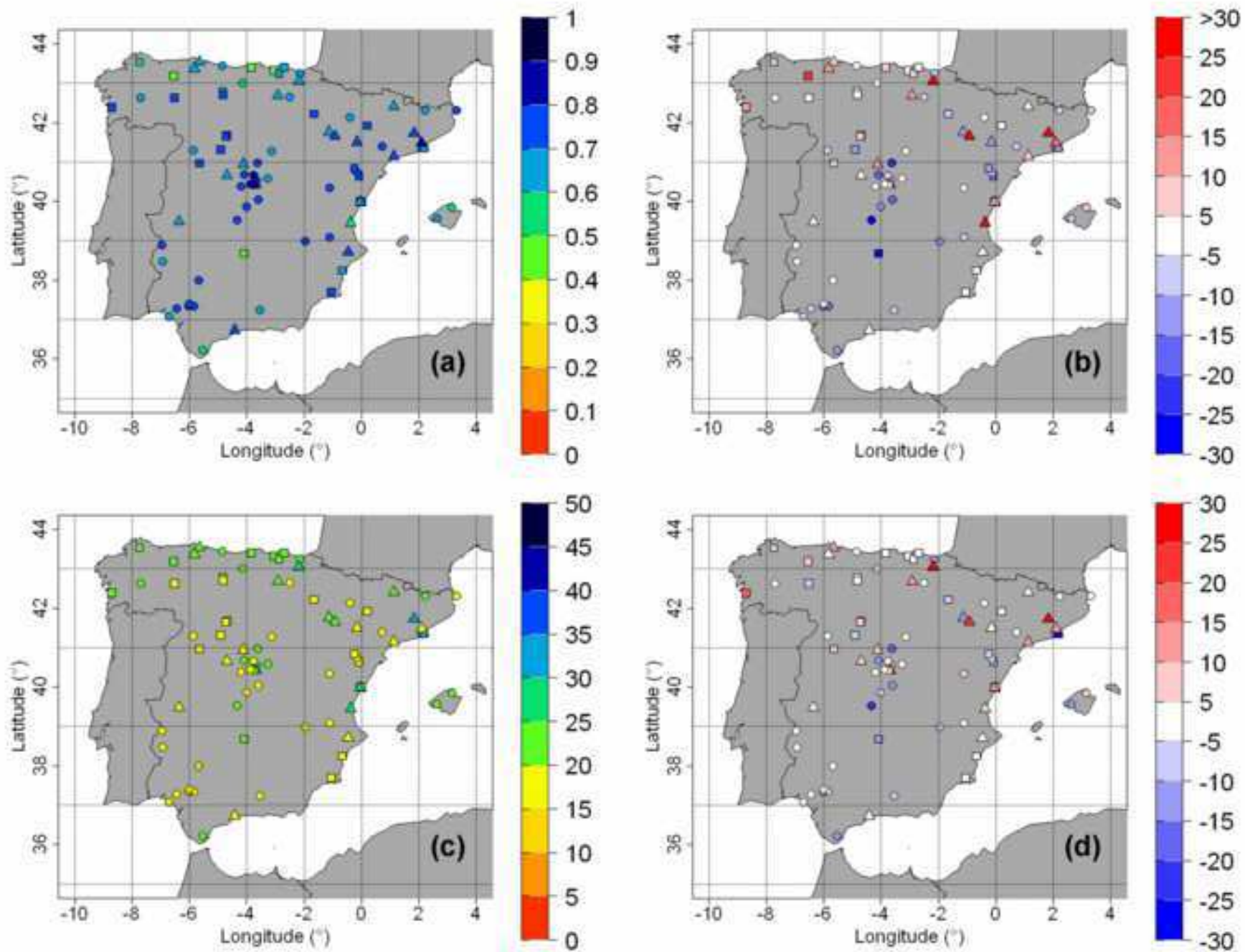


Figure 7

[Click here to download high resolution image](#)

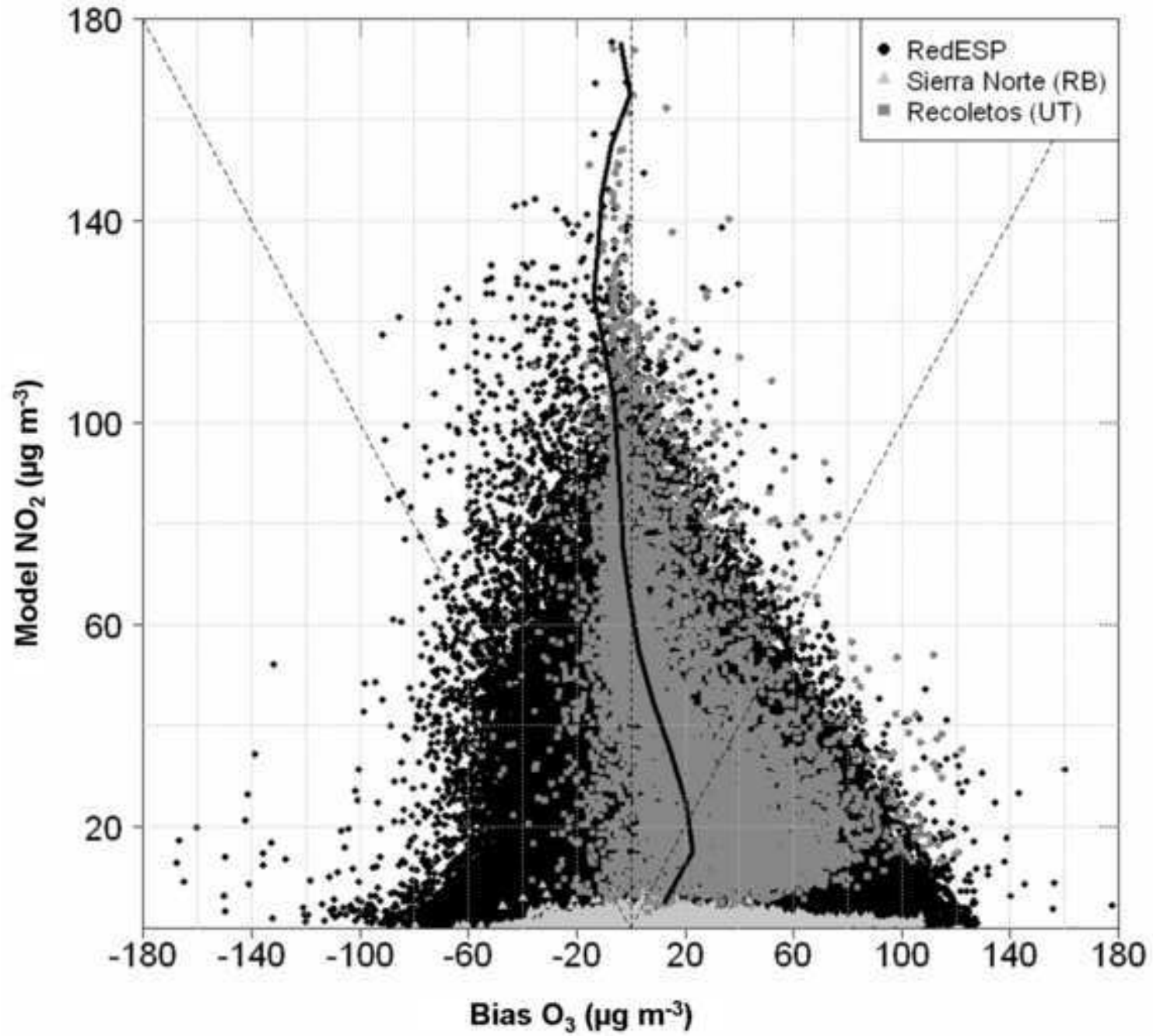


Figure 8

[Click here to download high resolution image](#)

